The Tenth Data Release of the Sloan Digital Sky Survey: First Spectroscopic Data from the SDSS-III Apache Point Observatory Galactic Evolution Experiment

Christopher P. Ahn[1], Carlos Allende Prieto[2,3], Scott F. Anderson[4], Timothy Anderton[1], Brett H. Andrews[5], Éric Aubourg[6], Stephen Bailey[7], Fabienne A. Bastien[8], Julian E. Bautista[6], Timothy C. Beers[9,10], Alessandra Beifiori[11], Chad F. Bender[12,13] Andreas A. Berlind[8], Florian Beutler[7], Vaishali Bhardwaj[4,7], Dmitry Bizyaev[14,15], Michael R. Blanton[16], Michael Blomqvist[17], John J. Bochanski[18,4], Adam S. Bolton[1], Arnaud Borde[19], Jo Bovy[20,21], W. N. Brandt[12,22], J. Brinkmann[14], Joel R. Brownstein[1], Nicolás G. Busca[6], William Carithers[7], Joleen K. Carlberg[23], S. Drew Chojnowski[24], Chia-Hsun Chuang[25], Johan Comparat[26], Justin R. Crepp[27], Rupert A.C. Croft[28], Antonio J. Cuesta[29], Katia Cunha[30,31], Luiz N. da Costa[32,33], Kyle S. Dawson[1], Nathan De Lee[8], Timothée Delubac[19], Rohit Deshpande[12], Saurav Dhital[34,8], Anne Ealet[35], Garrett L. Ebelke[14,15], Daniel J. Eisenstein[36], Courtney R. Epstein[5], Stephanie Escoffier[35], Massimiliano Esposito[2,3], D. Fabbian[2], Xiaohui Fan[31], Diane Feuillet[15], Nurten Filiz Ak[12,22,37], Scott W. Fleming[12,13], Andreu Font-Ribera[38,7], Peter M. Frinchaboy[39], J. G. Galbraith-Frew[1], D. A. García-Hernández[2,3], Ana E. García Pérez[24], Jian Ge[40], Bruce A. Gillespie[41,14], Léo Girardi[42,33], Jonay I. González Hernández[2], J. Richard Gott, III[43], James E. Gunn[43], Hong Guo[1], Samuel Halverson[12], David W. Harris[1], Sten Hasselquist[15], Suzanne L. Hawley[4], Michael Hayden[15], Frederick R. Hearty[24], Shirley Ho[28], Jon A. Holtzman[15], Klaus Honscheid[44,45], Joseph Huehnerhoff[14], Inese I. Ivans[1], Kelly M. Jackson[39,46], Peng Jiang[47,48], Jennifer A. Johnson[5,45], David Kirkby[17], K. Kinemuchi[14,15], Mark A. Klaene[14], Jean-Paul Kneib[49,26], Lars Koesterke[50], Dustin Lang[28], Jean-Marc Le Goff[19], Khee-Gan Lee[51], Daniel C. Long[14,15], Craig P. Loomis[43], Sara Lucatello[42], Robert H. Lupton[43], Bo Ma[40], Suvrath Mahadevan[12,13], Steven R. Majewski[24], A. Manchado[2,3], Marc Manera[52], Claudia Maraston[52], Sarah L. Martell[53], Cameron K. McBride[36], Ian D. McGreer[31], Brice Ménard[41,54,55], Sz. Mészáros[2,3], Jordi Miralda-Escudé[56,57], Antonio D. Montero-Dorta[1], Francesco Montesano[11], Demitri Muna[5], Adam D. Myers[58], Duy Cuong Nguyen[59], Robert C. Nichol[52], David L. Nidever[60,24], Pasquier Noterdaeme[61], Sebastián E. Nuza[62], Julia E. O'Connell[39], Robert W. O'Connell[24], Ross O'Connell[28], Matthew D. Olmstead[1], Daniel J. Oravetz[14], Russell Owen[4], Nathalie Palanque-Delabrouille[19], John K. Parejko[29], Isabelle Pâris[63], Joshua Pepper[64,8], Will J. Percival[52], Ignasi Pérez-Ràfols[57,65], Patrick Petitjean[61], Matthew M. Pieri[52], M. H. Pinsonneault[5], Francisco Prada[66,25,67], Adrian M. Price-Whelan[68], M. Jordan Raddick[41], Beth A. Reid[7,21], Jonathan C. Richards[1], Annie C. Robin[69], Natalie A. Roe[7], Ashley J. Ross[52], Nicholas P. Ross[7], Graziano Rossi[19],

Arpita Roy[12], Cristiano G. Sabiu[70], Ariel G. Sánchez[11], Conor Sayres[4], David J. Schlegel[7], Katharine J. Schlesinger[71], Sarah J. Schmidt[72], Donald P. Schneider[12,22], Mathias Schultheis[69], Kris Sellgren[5], Yue Shen[36,73], Matthew Shetrone[74], Yiping Shu[1], Audrey E. Simmons[14], M. F. Skrutskie[24], Anže Slosar[75], Verne V. Smith[9], Jennifer S. Sobeck[76], Keivan G. Stassun[8,77], Matthias Steinmetz[62], Michael A. Strauss[43,78], Alina Streblyanska[2,3], Molly E. C. Swanson[36], Ryan C. Terrien[12,13], Aniruddha R. Thakar[41], Daniel Thomas[52], Benjamin A. Thompson[39], Jeremy L. Tinker[16], Rita Tojeiro[52], Nicholas W. Troup[24], Jan Vandenberg[41], Mariana Vargas Magaña[28], Matteo Viel[79,80], Nicole P. Vogt[15], David A. Wake[81], Benjamin A. Weaver[16], David H. Weinberg[5], Benjamin J. Weiner[31], Martin White[82,7], John C. Wilson[24], John P. Wisniewski[83], W. M. Wood-Vasey[84,78], Christophe Yèche[19], Donald G. York[85], O. Zamora[2,3], Gail Zasowski[5,41], Idit Zehavi[86], Zheng Zheng[1], Guangtun Zhu[41]

[1] Department of Physics and Astronomy, University of Utah, Salt Lake City, UT 84112, USA.

[43] Department of Astrophysical Sciences, Princeton University, Princeton, NJ 08544, USA.

[2] Instituto de Astrofísica de Canarias (IAC), C/Vía Láctea, s/n, E-38200, La Laguna, Tenerife, Spain.

[3] Departamento de Astrofísica, Universidad de La Laguna, E-38206, La Laguna, Tenerife, Spain.

[4] Department of Astronomy, University of Washington, Box 351580, Seattle, WA 98195, USA.

[5] Department of Astronomy, Ohio State University, 140 West 18th Avenue, Columbus, OH 43210, USA.

[6] APC, University of Paris Diderot, CNRS/IN2P3, CEA/IRFU, Observatoire de Paris, Sorbonne Paris Cité, F-75205 Paris, France.

[7] Lawrence Berkeley National Laboratory, One Cyclotron Road, Berkeley, CA 94720, USA.

[UFRGS] Instituto de Física, UFRGS, Caixa Postal 15051, Porto Alegre, RS - 91501-970, Brazil.

[33] Laboratório Interinstitucional de e-Astronomia, - LIneA, Rua Gal.José Cristino 77, Rio de Janeiro, RJ - 20921-400, Brazil.

[9] National Optical Astronomy Observatory, 950 North Cherry Avenue, Tucson, AZ, 85719, USA.

[10] Department of Physics & Astronomy and JINA: Joint Institute for Nuclear Astrophysics, Michigan State University, East Lansing, MI 48824, USA.

[11] Max-Planck-Institut für Extraterrestrische Physik, Giessenbachstraße, D-85748 Garching, Germany.

[64] Department of Physics, Lehigh University, 16 Memorial Drive East, Bethlehem, PA 18015, USA.

[8] Department of Physics and Astronomy, Vanderbilt University, VU Station 1807, Nashville, TN 37235, USA.

[14] Apache Point Observatory, P.O. Box 59, Sunspot, NM 88349, USA.

[16] Center for Cosmology and Particle Physics, Department of Physics, New York University, 4 Washington Place, New York, NY 10003, USA.

[17] Department of Physics and Astronomy, University of California, Irvine, CA 92697, USA.

[18] Haverford College, Department of Physics and Astronomy, 370 Lancaster Avenue, Haverford, PA, 19041, USA.

[19] CEA, Centre de Saclay, Irfu/SPP, F-91191 Gif-sur-Yvette, France.

[20] Institute for Advanced Study, Einstein Drive, Princeton, NJ 08540, USA.

[21] Hubble fellow.

[55] Alfred P. Sloan fellow.

[12] Department of Astronomy and Astrophysics, 525 Davey Laboratory, The Pennsylvania State University, University Park, PA 16802, USA.

[22] Institute for Gravitation and the Cosmos, The Pennsylvania State University, University Park, PA

16802, USA.

[54] Kavli Institute for the Physics and Mathematics of the Universe (Kavli IPMU, WPI), Todai Institutes for Advanced Study, The University of Tokyo, Kashiwa, 277-8583, Japan.

[32] Observatório Nacional, Rua Gal. José Cristino 77, Rio de Janeiro, RJ - 20921-400, Brazil.

[81] Department of Astronomy, University of Wisconsin-Madison, 475 North Charter Street, Madison WI 53703, USA.

[62] Leibniz-Institut für Astrophysik Potsdam (AIP), An der Sternwarte 16, D-14482 Potsdam, Germany.

[49] Laboratoire d'Astrophysique, École Polytechnique Fédérale de Lausanne (EPFL), Observatoire de Sauverny, 1290, Versoix, Switzerland.

[26] Laboratoire d'Astrophysique de Marseille, CNRS-Université de Provence, 38 rue F. Joliot-Curie, F-13388 Marseille cedex 13, France.

[27] Department of Physics, 225 Nieuwland Science Hall, Notre Dame, IN, 46556, USA.

[79] INAF, Osservatorio Astronomico di Trieste, Via G. B. Tiepolo 11, I-34131 Trieste, Italy.

[80] INFN/National Institute for Nuclear Physics, Via Valerio 2, I-34127 Trieste, Italy.

[28] Bruce and Astrid McWilliams Center for Cosmology, Department of Physics, Carnegie Mellon University, 5000 Forbes Ave, Pittsburgh, PA 15213, USA.

[29] Yale Center for Astronomy and Astrophysics, Yale University, New Haven, CT, 06520, USA.

[56] Institució Catalana de Recerca i Estudis Avançats, Barcelona E-08010, Spain.

[57] Institut de Ciències del Cosmos, Universitat de Barcelona/IEEC, Barcelona E-08028, Spain.

[65] Departament d'Astronomia i Meteorologia, Facultat de Física, Universitat de Barcelona, E-08028 Barcelona, Spain.

[35] Centre de Physique des Particules de Marseille, Aix-Marseille Université, CNRS/IN2P3, E-13288 Marseille, France.

[15] Department of Astronomy, MSC 4500, New Mexico State University, P.O. Box 30001, Las Cruces, NM 88003, USA.

[52] Institute of Cosmology & Gravitation, Dennis Sciama Building, University of Portsmouth, Portsmouth, PO1 3FX, UK.

[36] Harvard-Smithsonian Center for Astrophysics, Harvard University, 60 Garden Street, Cambridge MA 02138, USA.

[31] Steward Observatory, 933 North Cherry Avenue, Tucson, AZ 85721, USA.

[UFRJ] Universidade Federal do Rio de Janeiro, Observatório do Valongo, Ladeira do Pedro Antônio 43, 20080-090 Rio de Janeiro, Brazil.

[37] Faculty of Sciences, Department of Astronomy and Space Sciences, Erciyes University, 38039 Kayseri,

Turkey.

[61] UPMC-CNRS, UMR7095, Institut d'Astrophysique de Paris, 98bis Boulevard Arago, F-75014, Paris, France.

[40] Department of Astronomy, University of Florida, Bryant Space Science Center, Gainesville, FL 32611-2055, USA.

[13] Center for Exoplanets and Habitable Worlds, 525 Davey Laboratory, Pennsylvania State University, University Park, PA 16802, USA.

[38] Institute of Theoretical Physics, University of Zurich, 8057 Zurich, Switzerland.

[39] Department of Physics & Astronomy, Texas Christian University, 2800 South University Drive, Fort Worth, TX 76129, USA.

[24] Department of Astronomy, University of Virginia, P.O.Box 400325, Charlottesville, VA 22904-4325, USA.

[42] INAF, Osservatorio Astronomico di Padova, Vicolo dell'Osservatorio 5, I-35122 Padova, Italy.

[86] Department of Astronomy, Case Western Reserve University, Cleveland, OH 44106, USA.

[45] Center for Cosmology and Astro-Particle Physics, Ohio State University, Columbus, OH 43210, USA.

[44] Department of Physics, Ohio State University, Columbus, OH 43210, USA.

[60] Dept. of Astronomy, University of Michigan, Ann Arbor, MI, 48104, USA.

[82] Department of Physics, University of California, Berkeley, CA 94720, USA.

[51] Max-Planck-Institut für Astronomie, Königstuhl 17, D-69117 Heidelberg, Germany.

[53] Australian Astronomical Observatory, PO Box 915, North Ryde NSW 1670, Australia.

[71] Research School of Astronomy & Astrophysics, Australian National University, Weston Creek, ACT, 2611, Australia.

[50] Texas Advanced Computer Center, University of Texas, 10100 Burnet Road (R8700), Austin, Texas 78758-4497, USA.

[73] Observatories of the Carnegie Institution of Washington, 813 Santa Barbara Street, Pasadena, CA 91101, USA.

[59] Dunlap Institute for Astronomy & Astrophysics, University of Toronto, Toronto, ON, M5S 3H4, Canada.

[41] Center for Astrophysical Sciences, Department of Physics and Astronomy, Johns Hopkins University, 3400 North Charles Street, Baltimore, MD 21218, USA.

[67] Instituto de Astrofísica de Andalucía (CSIC), Glorieta de la Astronomía, E-18080 Granada, Spain.

[58] Department of Physics and Astronomy, University of Wyoming, Laramie, WY 82071, USA.

[63] Departamento de Astronomía, Universidad de Chile, Casilla 36-D, Santiago, Chile.

[66] Campus of International Excellence UAM+CSIC, Cantoblanco, E-28049 Madrid, Spain.

ABSTRACT

The Sloan Digital Sky Survey (SDSS) has been in operation since 2000 April. This paper presents the tenth public data release (DR10) from its current incarnation, SDSS-III. This data release includes the first spectroscopic data from the Apache Point Observatory Galaxy Evolution Experiment (APOGEE), along with spectroscopic data from the Baryon Oscillation Spectroscopic Survey (BOSS) taken through 2012 July. The APOGEE instrument is a near-infrared $R \sim 22,500$ 300-fiber spectrograph covering 1.514–1.696μm. The APOGEE survey is studying the chemical abundances and radial velocities of 100,000 red giant stars in the bulge, bar, disk, and halo of the Milky Way. DR10 includes 178,397

---

[25] Instituto de Física Teórica, (UAM/CSIC), Universidad Autónoma de Madrid, Cantoblanco, E-28049 Madrid, Spain.

[68] Department of Astronomy, Columbia University, New York, NY 10027, USA.

[69] Université de Franche-Comté, Institut Utinam, UMR CNRS 6213, OSU Theta, Besançon, F-25010, France.

[70] School of Physics, Korea Institute for Advanced Study, 85 Hoegiro, Dongdaemun-gu, Seoul 130-722, Republic of Korea.

[75] Brookhaven National Laboratory, Bldg 510, Upton, NY 11973, USA.

[74] University of Texas, McDonald Observatory Hobby-Eberly Telescope 32 Fowlkes Rd McDonald Observatory, TX 79734-3005, USA.

[76] Department of Astronomy and Astrophysics and JUNA, University of Chicago, Chicago, IL 60637, USA.

[77] Department of Physics, Fisk University, 1000 17th Avenue North, Nashville, TN 37208, USA.

[78] Corresponding authors.

[84] PITT PACC, Department of Physics and Astronomy, University of Pittsburgh, Pittsburgh, PA 15260, USA.

[83] H.L. Dodge Department of Physics and Astronomy, University of Oklahoma, Norman, OK 73019, USA.

[85] Department of Astronomy and Astrophysics and the Enrico Fermi Institute, University of Chicago, 5640 South Ellis Avenue, Chicago, IL 60637, USA.

[23] Department of Terrestrial Magnetism, Carnegie Institution of Washington, 5241 Broad Branch Road, NW, Washington DC 20015, USA.

[47] Key Laboratory for Research in Galaxies and Cosmology, University of Science and Technology of China, Chinese Academy of Sciences, Hefei, Anhui, 230026, China.

[46] Department of Physics, University of Texas-Dallas, Dallas, TX 75080, USA.

spectra of 59,609 stars from APOGEE.

DR10 also roughly doubles the number of BOSS spectra over those included in the ninth data release. DR10 includes a total of 1,507,954 BOSS spectra, comprising 927,844 galaxy spectra; 182,009 quasar spectra; and 159,327 stellar spectra, selected over 6373.2 deg^2.

Subject headings: Atlases—Catalogs—Surveys

1. Introduction

The Sloan Digital Sky Survey (SDSS) has been in continuous operation since 2000 April. It uses a dedicated wide-field 2.5m telescope (Gunn et al. 2006) at Apache Point Observatory (APO) in the Sacramento Mountains in Southern New Mexico. It was originally instrumented with a wide-field imaging camera with an effective area of 1.5 deg^2 (Gunn et al. 1998), and a pair of double spectrographs fed by 640 fibers (Smee et al. 2013). The initial survey (York et al. 2000) carried out imaging in five broad bands (*ugriz*) to a depth of $r \sim 22.5$ over 11,663 deg^2 of high-latitude sky, and spectroscopy of 1.6 million galaxy, quasar, and stellar targets over 9380 deg^2. The resulting images were calibrated astrometrically (Pier et al. 2003) and photometrically (Ivezić et al. 2004; Tucker et al. 2006; Padmanabhan et al. 2008), and the properties of the detected objects were measured (Lupton et al. 2001). The spectra were calibrated and redshifts and classifications determined (Bolton et al. 2012). The data have been released publicly in a series of roughly annual data releases (Stoughton et al. 2002; Abazajian et al. 2003, 2004, 2005; Adelman-McCarthy et al. 2006, 2007, 2008; Abazajian et al. 2009; hereafter EDR, DR1, DR2, DR3, DR4, DR5, DR6, DR7, respectively) as the project went through two funding phases, termed SDSS-I (2000–2005) and SDSS-II (2005–2008).

In 2008, the SDSS entered a new phase, termed SDSS-III (Eisenstein et al. 2011), in which it is currently operating. It has four components. The Sloan Extension for Galactic Understanding and Exploration 2 (SEGUE-2), an expansion of a similar project carried out in SDSS-II (Yanny et al. 2009), used the SDSS spectrographs to obtain spectra of about 119,000 stars, mostly at high latitudes. The Baryon Oscillation Spectroscopic Survey (BOSS; Dawson et al. 2013) rebuilt the spectrographs to increase throughput, also increasing the number of fibers to 1000 (Smee et al. 2013). BOSS increased the imaging footprint of SDSS to 14,555 deg^2, and is obtaining spectra of galaxies and quasars to measure the baryon oscillation signatures in the clustering of matter as a cosmic yardstick to constrain cosmological models. The Multi-Object APO Radial Velocity Exoplanet Large-area Survey (MARVELS), which finished its data-taking in 2012, used a 60-fiber interferometric spectrograph to measure

high-precision radial velocities of stars, in order to search for planets and brown dwarfs. Finally, the Apache Point Observatory Galactic Evolution Experiment (APOGEE) uses a 300-fiber spectrograph to observe bright ($H < 13.8$ mag) stars in the H band at high resolution ($R \sim 22,500$) for accurate radial velocities and detailed elemental abundance determinations.

We have previously had two public data releases of data from SDSS-III. The Eighth Data Release (DR8; Aihara et al. 2011) included all data from the SEGUE-2 survey, as well as ~ 2500 deg^2 of new imaging data in the Southern Galactic Cap as part of BOSS. The Ninth Data Release (DR9, Ahn et al. 2012) included the first spectroscopic data from the BOSS survey: over 800,000 spectra selected from 3275 deg^2 of sky.

This paper describes the Tenth Data Release (hereafter DR10) of the SDSS survey. It includes almost 680,000 new BOSS spectra, covering an additional 3100 deg^2 of sky. It also includes the first public release of APOGEE spectra, with almost 180,000 spectra of almost 60,000 stars in a wide range of Galactic environments. As in previous SDSS data releases, DR10 is cumulative; it includes all data that were part of DR1–9. All data released with DR10 are publicly available on the SDSS-III website[1] and links from it.

The scope of the data release is described in detail in Section 2. We describe the APOGEE data in Section 3, and the new BOSS data in Section 4. The mechanisms for data access are described in Section 5. We conclude in Section 6.

2. Scope of DR10

DR10 presents the release of the first year of data from the SDSS-III APOGEE infrared spectroscopic survey and the first 2.5 years of data from the SDSS-III BOSS optical spectroscopic survey. In each case these data extend to the 2012 telescope shutdown for the summer monsoon season.

APOGEE was commissioned from 2011 May up through the summer shutdown in 2011 July. Survey-quality observations began 2011 Aug 31 (UTC-7), corresponding to Modified Julian Date (MJD) 55804. The APOGEE data presented in DR10 include all commissioning and survey-quality APOGEE data taken up to and including MJD 56121 (2012 July 13). The BOSS data include all data taken up to and including MJD 56107 (2012 June 29).

DR10 also includes the imaging data and spectroscopic data from SDSS-I/II and SDSS-

[1]http://www.sdss3.org/dr10/

III SEGUE-2, as well as the spectroscopy from the first year of BOSS, that were presented in DR9. Table 1 lists the contents of the data release, including the imaging coverage and number of plates and spectra of APOGEE and BOSS data. APOGEE plates are observed multiple times ("visits") to build signal-to-noise ratio (S/N) and to look for radial velocity variations; thus the number of spectra in DR10 is significantly larger than the number of stars observed. There are fewer repeat spectra in BOSS, but we also distinguish between the total number of spectra, and the number of unique objects observed. The imaging data, unchanged since DR8, also distinguishes between unique and total area and number of detected objects. The multiple repeat observations of the Equatorial Stripe in the Fall sky (Annis et al. 2011), used to search for Type Ia Supernovae (Frieman et al. 2008), dominate the difference between total and unique area imaged.

The footprints of the APOGEE and BOSS spectroscopic coverage in DR10 are shown in Figure 1 (Galactic coordinates) and Figure 2 (Equatorial coordinates), respectively. The distribution of SDSS-I/II and SEGUE-2 spectroscopy is not shown here; see the DR7 and DR8 papers. Note that the APOGEE fields are found both along the Galactic Plane, and at high Galactic latitudes to probe the halo. Note in particular the observations in the Galactic Center, which are observed at high airmass from APO. Because of the large and rapidly changing differential atmospheric refraction across the field of view at high airmass, these targets are chosen not over the full 7 deg^2 of each plate, but rather over a smaller region from 0.8–3.1 deg^2, as indicated by the smaller dots in Figure 1. The clump of points centered roughly at $l = 75°, b = +15°$ are special plates targeting *Kepler* satellite stars, as described in detail in § 3.4.

We should say something about the nature and quality of APOGEE commissioning data, either here or in Section 3.

The additional BOSS spectroscopy fills in most of the "doughnut" defined by the DR9 coverage in the North Galactic Cap. The DR10 BOSS sky coverage relative to the 10,000 deg^2 full survey region is described further in § 4.

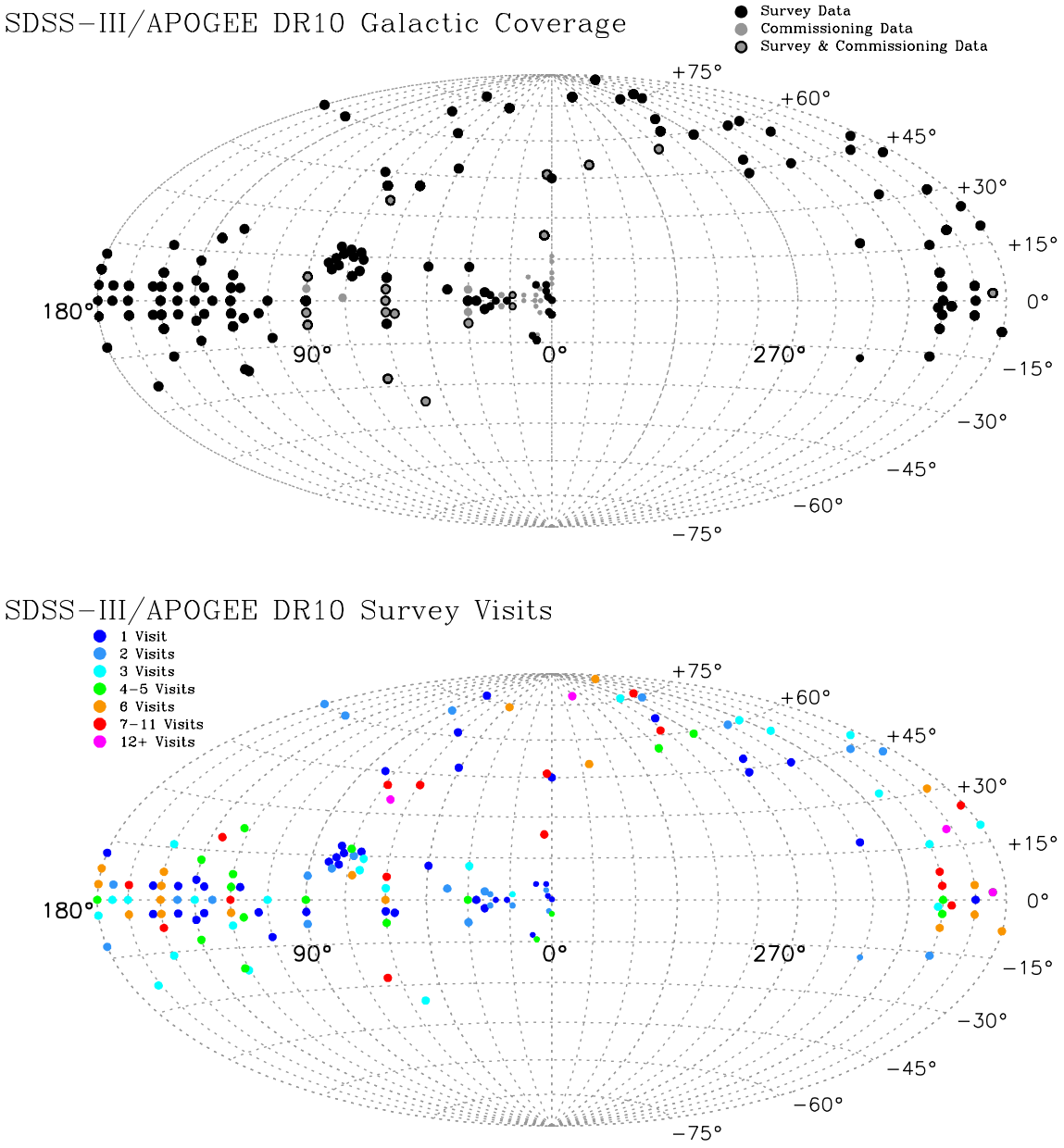

Fig. 1.— The distribution on the sky of all of the 232 APOGEE DR10 plates in Galactic coordinates: the Galactic Center is in the middle of the diagram. Each circle represents a plate. There are often several plates for a single location; there are a total of 170 locations shown. Smaller circles represent plates drilled over only a fraction of the 7 deg^2 focal plane to minimize differential atmospheric refraction. Note the distribution of points along the Galactic Plane. The concentration of plates at $l = 75°, b = +15°$ is a special program targeting stars observed by the *Kepler* telescope; see § 3.4. (top) Distribution of plates in both the commissioning phase and survey phase (both are included in DR10). (bottom) Plates distinguished by the number of visits obtained by DR10 in the survey phase.

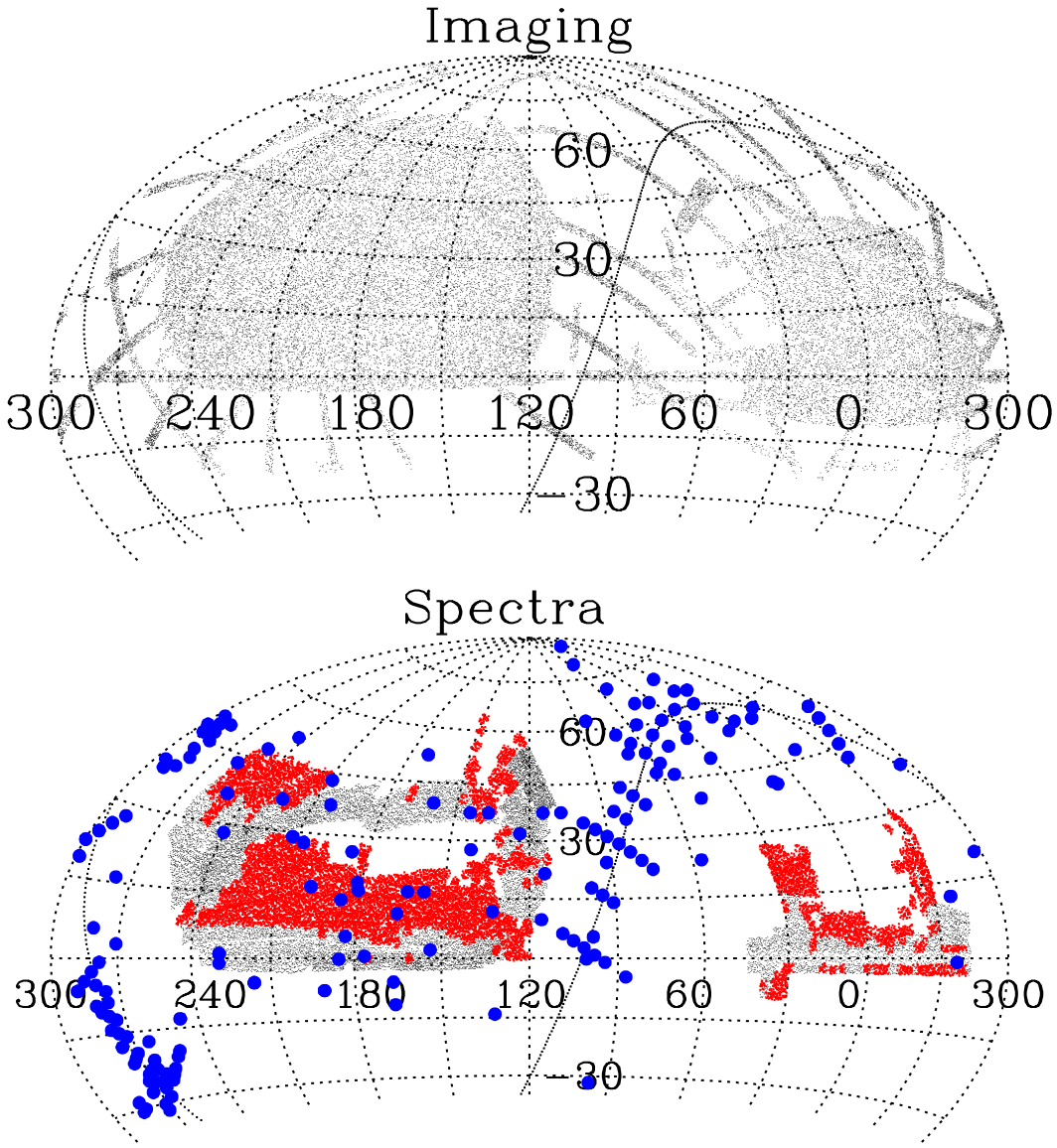

Fig. 2.— The distribution on the sky of all SDSS imaging (top; 14,555 deg^2 – same as DR8 and DR9) and BOSS and APOGEE DR10 spectroscopy (6373.2 deg^2) in equatorial coordinates ($\alpha = 0°$ is the right of center in this projection). Grey shows regions included in DR9; the increment included in DR10 is in red. The blue shows the position of the APOGEE plates included in DR10. The Galactic Plane is shown by the dotted line. The Northern Galactic Cap is on the left of the figure, and the Southern Galactic Cap on the right. The BOSS sky coverage is actually constructed using a random subsample of the BOSS DR10Q quasar catalog (Pâris et al. 2013). Note that the sky below $\delta < -30°$ is never above an airmass of 2.0 from APO (latitude=32°46′49″N).

Table 1. Contents of DR10

Optical Imaging[a]		
	Total	Unique[b]
Area Imaged	31637 deg^2	14555 deg^2
Cataloged Objects	1231051050	469053874

APOGEE Spectroscopy			
	Commissioning	Survey	Total
Plate-Visits	98	586	684
Plates	51	232	281
Pointings	43	150	170
	Spectra	Stars	
All Stars	178397	59609	
Stars with > 3 visits	···	29701	
Stars with > 12 visits	···	923	
Stars with S/N per resolution element > 100	···	47675	
Stellar parameter calibration stars	5178	1065	
Radial velocity calibration stars	162	16	
Telluric line calibration stars	24283	7003	
Ancillary program objects	8894	3344	

BOSS Spectroscopy		
	Total	Unique[b]
Spectroscopic footprint effective area	···	6373.2 deg^2
Plates[c]	1515	1489
Optical Spectra observed[d]	1507954	1391792
All Galaxies	927844	859322
CMASS galaxies	612195	565631
LOWZ galaxies	224172	208933
All Quasars	182009	166300

Table 1—Continued

Main Quasars[e]	159808	147242
Main Quasars, $2.15 < z < 3.5$[f]	114977	105489
Ancillary program spectra	72184	65494
Stars	159327	144968
Standard stars	30514	27003
Sky spectra	144503	138491
Unclassified spectra[g]	101550	89003
All Optical Spectroscopy from SDSS up through DR10		
Total number of spectra	3358200	
Total number of useful spectra[h]	3276914	
Galaxies	2428961	
Quasars	308377	
Stars	736484	
Sky	247549	
Unclassified[g]	138663	

[a]These numbers are unchanged since DR8.

[b]Removing all duplicates, overlaps, and repeat visits from the "Total" column.

[c]Twenty-six plates of the 1515 observed plates were re-plugged and re-observed for calibration purposes. Six of the 1489 unique plates are different drillings of the same tiling objects.

[d]This excludes the small fraction of the observations through fibers that are broken or that fell out of their holes after plugging. There were 1,515,000 spectra attempted.

[e]This counts only quasars that were targeted by the main quasar survey (Ross et al. 2012), and thus does not include those from ancillary programs (Dawson et al. 2013).

[f]Quasars with redshifts in the range $2.15 < z < 3.5$ provide the most signal in the BOSS spectra of the Ly-α forest.

[g]Non-sky spectra for which the automated redshift/classification pipeline (Bolton et al.

2012) gave unreliable results, as indicated by the ZWARNING flag.

[h]Spectra on good or marginal plates. "Spectrum" refers to a combined set of sub-exposures that define a completed plate.

[h]Spectra on good or marginal plates.

3. The Apache Point Observatory Galaxy Evolution Experiment (APOGEE)

3.1. Overview of APOGEE

Stellar spectra of red giants show a rich range of absorption lines from a wide variety of elements in the H band (1.5–1.8μm). At these long wavelengths, the absorption due to dust in the plane of the Milky Way is much reduced, meaning that a high-resolution study of stars in the H band will allow studies of all components of the Milky Way, from the disk and bulge to the halo.

APOGEE's goal is to trace the history of star formation in, and the assembly of, the Milky Way. It is doing this by observing 100,000 red giant stars throughout the galaxy. Using an infrared multi-object spectrograph with a resolution of $R \sim 22{,}500$, APOGEE can survey the halo, disk, and bulge+bar in a much more uniform fashion than previous surveys. APOGEE takes advantage of the fiber infrastructure on the SDSS telescope, using 300 fibers, each subtending $2''$ on the sky, distributed over the full 7 deg^2 field of view[2]. The light from the fibers falls onto three HAWAII-2RG 2K $\times$ 2K infrared detectors (Garnett et al. 2004), covering the wavelength range from 1.514μm to 1.696μm, with two gaps (see Section 3.2 for details). APOGEE targets are chosen with magnitude and color cuts from the data of the Two-Micron All-Sky Survey (2MASS; Skrutskie et al. 2006), with most stars brighter than $H = 13.8$ mag (on the 2MASS Vega-based system).

The high resolution of the spectra allow accurate radial velocities with a typical uncertainty of 100 meters sec^{-1} and detailed chemical abundance determinations for up to 15 elements. The radial velocity data are being used to explore the kinematic structure of the Milky Way and its substructures, and to constrain dynamical models. The chemical abundance data will allow studies of the chemical evolution of the Galaxy and the history of star formation. The combination of kinematic and chemical data will allow important new constraints on the formation history of the Milky Way.

A full overview of the APOGEE survey will be presented in Majewski et al. (2013). The APOGEE instrument will be detailed in Wilson et al. (2013) and is summarized here in Section 3.2. The target selection process for APOGEE is described in Zasowski et al. (2013) and is described in brief here in Section 3.3. In Section 3.4 we describe a unique cross-calibration program between SDSS-III APOGEE spectra of stars observed and astro-

[2]Plates observed at high airmass, especially near the Galactic Center, have targets over a smaller area on each plate to minimize differential atmospheric refraction.

seismology measurements of stars from data from the NASA *Kepler* telescope[3] (Gilliland et al. 2010). Section 3.5 describes the pipeline that extracts calibrated spectra for each star from the two-dimensional spectrographs (Nidever et al. 2013) and Section 3.6 describes the pipeline that measures stellar parameters and chemical abundances for each star (Shetrone et al. 2013; Garcia-Perez et al. 2013; Mészáros et al. 2013). Section 3.7 summarizes the APOGEE data products available in DR10. Important caveats about APOGEE data that potential users should be aware of are described in Section 3.8.

3.2. The APOGEE Instrument and Observations

All previous SDSS spectroscopic data (EDR and DR1–DR9), including all SEGUE and SEGUE-2 data, were taken with optical spectrographs. In Data Release 10, we release the first near-infrared spectra from APOGEE.

APOGEE spectra are quite different from previous SDSS spectra: they are obtained in the infrared portion of the electromagnetic spectrum, covering wavelengths between 1.514 and 1.696 microns. Additionally, the spectra are taken at significantly higher spectral resolution, allowing the determination of more accurate radial velocities and detailed information about the stellar atmospheres of the survey stars.

The APOGEE spectrograph measures 300 spectra in a single observation; roughly 230 science targets, 35 on blank areas of sky to measure telluric emission, and 35 hot blue stars to calibrate atmospheric absorption. This multiplexing is done by means of the same aluminum plates and fiber optic technology as have been used for the optical spectrograph surveys of SDSS. Each plate corresponds to a specific patch of sky, and is pre-drilled with holes corresponding to the sky positions of objects in that area, meaning that each area requires one or more unique plates.

The APOGEE spectrograph uses three detectors to cover the H-band range, "blue": 1.514–1.581μm, "green": 1.585–1.644μm, and "red" 1.647–1.696μm. There are thus two gaps each a few nm wide in the spectra. The detectors are mildly under-sampled, with roughly 1.6–2.3 pixels per resolution element (FWHM; increasing from blue to red across the detectors). Figure 4 shows the results of a typical exposure. Clean up figure order. Each observation consists of an "AB" pair of exposures for a given pointing on the sky, with the detector array offset by 0.5 pixels along the dispersion direction between the two exposures. This dithering technique, common to infrared observations, separates effects of the detector

[3]http://kepler.nasa.gov/

(which remain fixed during a dither) and the astrophysical signal (which shifts). This well-controlled sub-pixel dithering allows the derivation of combined properly sampled spectra from the individual under-sampled exposures. The actual spectral resolution as a function of wavelength is provided as a Gauss-Hermite function for each APOGEE spectrum in DR10.

APOGEE stars are observed over multiple visits to achieve the planned S/N and to identify binary systems from variations in radial velocities. Figure 8 shows the distribution of number of visits of observations included in DR10; most stars have three or fewer visits, although this distribution will broaden with the final data release. These visits are separated across different nights and often different seasons, allowing us to look for radial velocity variability. The distribution of time intervals between visits is shown in Figure 9, with peak at one and two lunations (30 and 60 days) A typical observation strategy is an "ABBA" sequence of four 15-minute exposures to reach the target S/N for a given observation. The combination of all "AB" and "BA" pairs for a given plate during a night is called a "visit." The visit is the basic product for what are considered individual spectra for APOGEE.

Each visit is uniquely identified by the plate number and MJD of the observation. Plates are generally re-plugged between observations, so while "plate+MJD+fiber" remains a unique identifier in APOGEE spectra as it is in optical SDSS spectra, "plate+fiber" does not refer to the same object across all visits. The spectra from all visits are co-added to produce the aggregate spectrum of the star. The final co-added spectra are processed by the in-depth stellar parameters pipeline described in § 3.6.

The aim is for a final coadded spectrum of each star with a S/N of > 100 per resolution element. The DR10 data include some stars that have yet to receive their full complement of visits, and thus have significantly lower quality spectra. Figures 6 and 7 show the distribution of S/N; not surprisingly, S/N is strongly correlated with the brightness of the star. Future data releases will include additional visits for these stars and a consequent increase in total co-added S/N and more refined stellar parameters.

The APOGEE plates are drilled with the same plate-drilling machines used for BOSS, and the plate numbers are sequential. This scheme means that that the BOSS and APOGEE plate numbers are interleaved and that no plate number is assigned to both a BOSS and APOGEE plate.

3.3. APOGEE Main and Ancillary Targets

APOGEE main targets are selected from 2MASS data (Skrutskie et al. 2006) using apparent magnitude limits to meet the S/N goals and a dereddened color cut of $(J - K_s)_0 >$

0.5 mag to identify red giants in multiple components of the galaxy: the disk, bulge, and halo. This selection results in a sample of objects that are predominantly red giant stars with $4500 < T_{\rm eff} < 5200$ K and $\log_{10} g < 3.5$. APOGEE has also implemented a number of ancillary programs to pursue specific investigations enabled by this instrument. The selection of the main target sample and the ancillary programs, together with the bit flags that can be used to identify why an object was targeted for spectroscopy, are described in detail in Zasowski et al. (2013). In DR10, APOGEE stars are named based on their 2MASS ID (i.e., '2M', followed by the position)[4].

The corrections to 2MASS colors for Galactic extinction can be quite significant at low Galactic latitude. They are based on the *Spitzer* IRAC GLIMPSE survey (Benjamin et al. 2003; Churchwell et al. 2009) and the Wide-field Infrared Survey Explorer(WISE; Wright et al. 2010) $\lambda = 4.5\mu$m data following the Rayleigh-Jeans Color Excess Method described in Majewski et al. (2011) and Zasowski et al. (2013) using the color extinction curve from Indebetouw et al. (2005). Fig. 3 shows the measured and reddening-corrected JHK_s color-color and magnitude-color diagrams for the APOGEE stars included in DR10.

Exceptions to the $(J - K_s)_0 > 0.5$ mag color limit that appear in DR10 include the telluric calibrator stars, early-type stars targeted in well-studied open clusters, stars observed on commissioning plates that did not employ the color limit, and stars in sparsely populated halo fields for which adopted a bluer color limit of $(J - K_s)_0 > 0.3$ mag in order to fill all of the fibers. Ancillary program targets may also have colors and magnitudes beyond the limits of APOGEE's normal red giant sample.

While the majority of observable main sequence stars are intrinsically bluer than $(J - K_s) < 0.5$ mag, highly extincted main sequence stars can have observed colors that overlap the red giant locus. Dereddening the apparent magnitudes produces a clear separation between these populations and allows APOGEE to efficiently target the more distant red giant stars.

3.4. APOKASC

Non-radial oscillations are detected in virtually all red giants targeted by the *Kepler* satellite (Borucki et al. 2010; Hekker et al. 2011), and the observed frequencies are sensitive diagnostics of basic stellar properties such as mass, radius, and age (for a review, see Chaplin

[4]2MASS IDs as presented in DR10 are somewhat abbreviated: "2M21504373+4215257" is stored for the formal designation "2MASS 21504373+4215257".

et al. 2013).

There are significant opportunities afforded by the combination of *Kepler* asteroseismological measurements with APOGEE chemical abundance measurements. "APOKASC" is a collaboration between SDSS-III and the *Kepler* Asteroseismology Science Collaboration (KASC), which is obtaining APOGEE spectra for $\sim 10,000$ stars in fields observed by the *Kepler* satellite (see Figure 1). The joint measurement of masses, radii, ages, evolutionary states, and chemical abundances for all these stars will enable investigations of Galactic stellar populations and fundamental stellar physics.

DR10 presents 4,204 spectra of 2,308 stars of the anticipated final APOKASC sample. Asteroseismic data from the APOKASC collaboration was used to calibrate the APOGEE spectroscopic surface gravity results for all APOGEE stars presented in DR10 (Mészáros et al. 2013). A joint asteroseismic and spectroscopic value-added catalog will be released separately (Pinsonneault et al. 2013).

3.5. APOGEE Data Analysis

The APOGEE data processing has two major components: (1) the basic data extraction pipeline that removes effects of the detector and produces calibrated one-dimensional spectra; (2) the analysis pipeline that takes these one-dimensional spectra and calculates stellar properties and elemental abundances – the APOGEE Stellar Parameters and Chemical Abundances Pipeline (ASPCAP). We summarize the first of these in this section, and ASPCAP in § 3.6.

The extraction of one-dimensional coadded spectra will be fully described in Nidever et al. (2013). We provide here a brief summary to help the reader understand how individual APOGEE exposures are processed. A 15-minute APOGEE exposure actually consists of a series of non-destructive readouts every 10.7 seconds that result in a three-dimensional data cube. The first step in processing is to extract a two-dimensional image from a combination of these measurements. After bias subtraction, the "up-the-ramp" values for each pixel are fit to a line to derive the count rate for that pixel. Cosmic rays create tell-tale jumps in the "up-the-ramp" signal, which are easily recognized, removed, and flagged for future reference. The count rate in each pixel is multiplied by the exposure time to obtain a two-dimensional image. These two-dimensional images are then dark-subtracted and flat-fielded. One-dimensional spectra are extracted simultaneously for the entire set of 300 fibers based on wavelength and profile fits from flat-field calibration images. Wavelength calibration is based on observations of arc lamps, as adjusted by the location of night sky lines.

The individual exposure spectra are then corrected for telluric absorption and emission based on the sky spectra and standard star spectra, and combined accounting for the dither offset between each "A" and "B" exposure. This combined visit spectrum is flux calibrated based on a model of the APOGEE instrument's response from lab-based observations of a blackbody. The spectrum is then scaled to match the 2MASS measured apparent H-band magnitude. A preliminary radial velocity is estimated for the visit spectrum based on a pre-computed grid of synthetic stellar spectra, and is stored with the individual visit spectrum.

In addition to the individual visit spectra, the APOGEE software pipeline coadds the spectra from different visits to the same field, yielding a higher S/N spectrum of each object. Figure 5 shows typical flux-calibrated coadded spectrum from APOGEE. Make sure the figure is actually a flux-calibrated spectrum This higher S/N spectrum is then normalized to unit continuum and refit for the stellar parameters (as we describe in § 3.6), and updated radial velocities for the individual visits are re-calculated based on the stellar parameters from the coadded spectrum. These combined spectra are identified by the 2MASS catalog name of each star.

3.6. APOGEE Stellar Parameter and Chemical Abundances Pipeline (ASPCAP)

The ultimate goal of APOGEE is to determine the effective temperature, surface gravity, metallicity, and detailed chemical abundances for APOGEE stars. Stellar parameters and chemical abundances are extracted from the continuum-normalized coadded APOGEE spectra by comparing with synthetic spectra calculated using state-of-the-art model photospheres (Mészáros et al. 2012) and atomic and molecular line opacities (Shetrone et al. 2013).

Such fits to high-resolution data are traditionally done by hand. However, given the sheer size of APOGEE's spectral database, automatic analysis methods had to be implemented. For that purpose, ASPCAP searches the best fitting spectrum through chi-squared minimization within a pre-computed multi-dimensional grid of synthetic spectra. The output parameters of the analysis are effective temperature ($T_{\rm eff}$), surface gravity ($\log_{10} g$), metallicity ([M/H]), and the relative abundances of α elements ([α/M]), carbon ([C/M]), and nitrogen ([N/M]). Figure 10 shows examples of model fits to APOGEE spectra. Describe the figure further once it is put in ASPCAP will be fully described in an upcoming paper (Garcia-Perez et al. 2013).

Chemical composition parameters are defined as follows. The abundance of a given

element X is defined relative to solar values in the standard way:

$$[X/H] = \log_{10}(n_X/n_H)_{\rm star} - \log_{10}(n_X/n_H)_{\odot} \quad (1)$$

where n_X and n_H are respectively the numbers of atoms of element X and hydrogen, per unit volume, in the stellar photosphere. The parameter [M/H] is defined as an overall metallicity scaling, assuming the solar abundance pattern. The deviation of the abundance of element X from that pattern is given by:

$$[X/M] = [X/H] - [M/H] \quad (2)$$

The α elements considered in the APOGEE spectral libraries are O, Ne, Mg, Si, S, Ca, and Ti, and [α/H] is defined as an overall scaling of the abundances of those elements, where they are assumed to vary together while keeping their relative abundances fixed at solar values. For DR10, we allow four metallicity parameters to vary: the overall metallicity, and the abundances of α elements, carbon, and nitrogen. Carbon and nitrogen contribute significantly to the opacity in APOGEE spectra of cool giants, particularly in the form of molecular lines due to OH, CO, and CN, while there are numerous atomic lines due to α elements other than oxygen.

Mészáros et al. (2013) have verified the outputs of ASPCAP by comparing with results of high-resolution spectroscopy in the literature for for stars targeted by APOGEE in open and globular clusters spanning a wide range in metallicity. These comparisons uncovered small systematic differences between ASPCAP and literature results; we have applied offsets to bring the two into agreement. With these offsets in place, the APOGEE metallicities are accurate to within 0.1 dex for stars of S/N $>$ 100 per resolution element that lie within a strict range of $T_{\rm eff}$, $\log_{10} g$, and [M/H] (see Mészáros et al. 2013, for details). Can we state what this range is, understanding that it may be a bit complicated??? APOGEE mean values per cluster of [α/M] are in good agreement with those in the literature. However, there are systematic correlations between [α/M] and both [M/H] and $T_{\rm eff}$ for stars outside the range $-1.0 \leq$ [M/H] ≤ 0.0. Moreover, important systematic effects may be present in [α/M] for stars cooler than $T_{\rm eff} \sim 4200$ K, so we discourage use of [α/M] in that regime. Finally, comparison with literature values for carbon and nitrogen abundances shows large scatter and significant systematic differences. In view of the relative paucity and uncertainty of literature data for these elements, more work is needed to understand these systematic and random differences before APOGEE abundances for carbon and nitrogen can be safely adopted in science applications.

Figures 11 and 12 show the distribution of stellar properties derived by ASPCAP for stars included in DR10. The calibration of the ASPCAP models extends from $3610 < T_{\rm eff} < 5255$ K, so while the lower limit is predominantly due to population selection effects (there are

relatively few stars with $T_{\rm eff} < 3500$ K that are brighter than $H = 13.8$ mag) this lower limit to $T_{\rm eff}$ is also the limit of the model. All stars lie in the range $3610 < T_{\rm eff} < 5255$ K, with a peak at about 4800 K. The surface gravity distribution peaks at $\log_{10} g \sim 2.5$, corresponding to red giants, and is strongly correlated with surface temperature The ASPCAP models are calibrated from $-0.5 < \log_{10} g < 3.6$, which is reflected in the range shown. The metallicity distribution peaks just below subsolar levels, with a tail extending from [M/H] ~ -0.5 to below -2.3. Check the `APOGEE_ASPCAPFLAG` values to identify stars near the edges of the model parameter grid. The α abundance is bimodal. What does this reflect? Different stellar populations?

3.7. APOGEE Data Products

The APOGEE data as presented in DR10 are available as the individual 15-minute spectra taken on a per-exposure basis (organized either by object or by plate+MJD+fiber), as combined co-added spectra on a per-object basis, and normalized to unit continuum as analyzed by the APOGEE pipeline (ASPCAP) to compute stellar properties. The DR10 Catalog Archive Server (CAS) provides the stellar parameters (including the radial velocity) from the APOGEE spectra on a per-visit and a co-added star basis. The individual raw exposure files, processed spectra, and combined summary files of stellar parameters are provided as FITS[5] files (Wells et al. 1981) through the DR10 Science Archive Server (SAS).

3.8. Important information about APOGEE spectra

When working with APOGEE data, users should be aware of several features and potential issues with the data. This is the first data release for APOGEE; the handling of some of these issues in the pipelines may be improved in subsequent data releases.

Many of these issues are documented in the data by the use of bitmasks that flag various conditions. For the APOGEE spectral data, there are two bitmasks: `APOGEE_PIXMASK`, which flags conditions at a pixel-by-pixel level, and `APOGEE_STARFLAG`, which flags conditions at the full spectrum level.

Some of the more important features to be aware of include:

Gaps in the spectra: There are gaps in the spectra corresponding to the the regions

[5]http://fits.gsfc.nasa.gov/

that fall between the three detectors. In addition to these, gaps arise because the infrared arrays have a moderate number of bad or hot pixels for which useful data are not available. As multiple dithered exposures are combined to make a visit spectrum, values from missing regions are needed to calculate the dither-combined signal in nearby pixels; as a result, these nearby pixels are also marked as bad in `APOGEE_PIXMASK`. This leads to apparent gaps of bad pixels in the combined visit spectra, since the current pipeline conservatively sets the spectral data for these pixels to zero. Generally, the bad pixels affect neighboring pixels only at a very low level, and the data may be usable; in subsequent data releases, we will preserve more of the data, while maintaining the conservative identification of potential bad pixels in the pixel mask.

Imperfect Night-Sky-Line Subtraction: The Earth's atmosphere has strong emission in OH lines in the APOGEE bandpass. At the location of these lines, the sky flux is many times brighter than the stellar flux for all except the brightest stars. Even if the sky subtraction algorithm were perfect, the photon noise at the positions of these sky lines would dominate the signal, so there is little useful information at these wavelengths. With this in mind, we did not put in very much effort into optimizing the subtraction, and as a result, the spectra in these regions can show significant sky line residuals. These regions are masked for the stellar parameter analysis so that they do not impact the results. The affected pixels have the `SIG_SKYLINE` bit set in `APOGEE_PIXMASK`.

Error arrays don't track correlated errors: APOGEE spectra from an individual visit are made by combining multiple individual exposures taken at different dither positions. Because the dithers are not spaced by *exactly* 0.5 pixels, there is some correlation between pixels that is introduced when combined spectra are produced. The error arrays for the visit spectra do not include information about these correlations. In the visit spectra, these correlations are generally small since the dither mechanism is quite accurate. However, when multiple visit spectra are combined to make the final combined spectra, they must be re-sampled onto a common wavelength grid, taking into account the different barycentric velocities of each individual visit. This re-sampling introduces significant additional correlated errors between adjacent pixels that are also not tracked in the error arrays. How strong is this correlation?

Error arrays don't include systematic error floors: The errors that are reported for each spectrum are derived based on propagation of Poisson and readout noise. However, based on observations of bright hot stars, we believe that other, possibly systematic, uncertainties currently limit APOGEE observations to a maximum S/N of ~ 200. The error arrays published in DR10 currently report the estimated errors without any contribution

from a systematic component. However, for the ASPCAP analysis, we impose an error floor corresponding to 0.5% of the continuum level.

Fiber crosstalk: While an effort is made not to put faint stars adjacent to bright ones on the detector, this occasionally occurs. We flag objects (in `APOGEE_STARFLAG`) with a `BRIGHT_NEIGHBOR` flag if an adjacent star is > 10 times brighter than the object, and with a `VERY_BRIGHT_NEIGHBOR` flag if an adjacent star is > 100 time brighter; the latter exposures are marked as bad and not used in combined spectra.

Persistence in the "blue" chip: There is a known "superpersistence" in 1/3 of the region of the "blue" APOGEE chip (1.514μm$< \lambda < 1.581\mu$m), and to a lesser extent in some regions of the "green" chip, whereby some of the charge from previous exposures persists in subsequent exposures. Thus the values read out in these locations depend on the previous exposure history for that chip. The effect of superpersistence can vary significantly, but residual signal can amount to as much as 10–20% of the signal in a previous exposure. How much of an effect this has depends on the brightness of the source in a given exposure relative to the brightness of sources in previous exposures. The current pipeline does not attempt to correct for this effect; any such correction is likely to be rather complex. For the current release, pixels known to be affected by persistence are flagged in `APOGEE_PIXMASK` at three different levels (`PERSIST_LOW, PERSIST_MEDIUM, PERSIST_HIGH`). Spectra that have significant numbers of pixels ($> 20\%$ of total pixels) that fall in the persistence region have comparable bits set in the `APOGEE_STARFLAG` bitmask to warn that the spectra for these objects may be contaminated. In a few cases, the effect of persistence is seen dramatically as an elevated number of counts in the blue chip relative to the other chips; these are flagged as `PERSIST_JUMP_POS` in `APOGEE_STARFLAG`. We are still actively investigating the effect of persistence on APOGEE spectra and derived stellar parameters, and are working on corrections.

ASPCAP analysis-level flags:

Needs to be written. HOLTZMAN is working on this

4. The Baryon Oscillation Spectroscopic Survey (BOSS)

The BOSS survey is described in detail in Dawson et al. (2013), and the instrument is described in Smee et al. (2013). BOSS is obtaining spectra of 1.5 million galaxies (Ahn et al. 2012), and 150,000 quasars with redshifts between 2.15 and 3.5 (Ross et al. 2012), selected from 10,000 deg^2 of SDSS imaging data. The large-scale distribution of galaxies, and the structure in the quasar Lyman α forest, allow measurements of the baryon oscillation

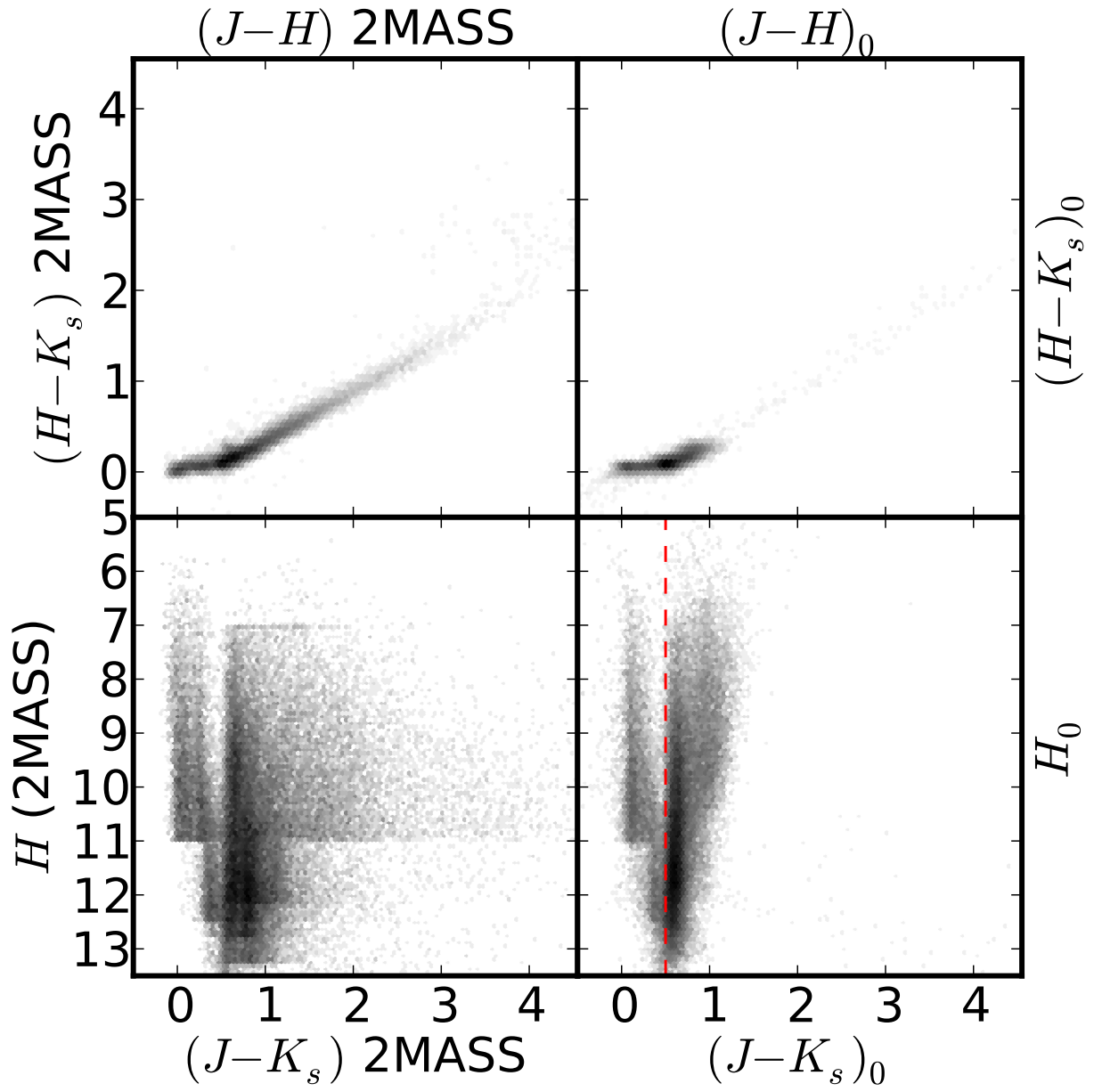

Fig. 3.— 2-dimensional hexagonal-binned histogram of the APOGEE DR10 stars in (top) 2MASS JHK_s color space; and (bottom) 2MASS H vs. $J-K_s$. The left column is observed magnitude from 2MASS, while the right column has been dereddened based on $J-4.5\mu$m color as in Zasowski et al. 2013. The vertical dashed line at $(J-K_s)_0 = 0.5$ shows the selection of the main APOGEE red giant sample; bluer objects include telluric calibration stars as well as other special program targets. The grey scale is logarithmic. MWV: Ensure use of consistent Color map scale.

signature as a function of redshift (Anderson et al. 2012, 2013; Busca et al. 2013). In addition, about 5% of the fibers are devoted to a series of ancillary programs with a broad range of science goals (see the Appendix of Dawson et al. 2013).

DR9 included about 830,000 BOSS spectra over 3275 deg^2; DR10 adds an additional 679,000 spectroscopic observations over 3100 deg^2. The quality of the data is essentially unchanged from DR9. The spectra cover the wavelength range 3650–10,400Å, with a resolution of roughly $R \sim 1800$. The S/N is of course a strong function of magnitude, but at a model magnitude of $i = 19.9$, the magnitude limit of the CMASS galaxy sample, the typical median S/N per pixel across the spectra is about 2. The majority of these spectra are of adequate quality for classification and measurement of a redshift; only 6% of the galaxy target spectra, and 12% of the quasar target spectra, are flagged by the pipeline (Bolton et al. 2012) as having uncertain classification.

Figure 13 shows the sky coverage of the BOSS spectroscopic survey in more detail than in Figure 2. The tiling of the individual circular plates is visible in this completeness map of the CMASS galaxy sample. Because of the finite extent of the cladding around fibers, no two fibers can be placed closer than 62″, meaning that spectroscopy will be only about 94% complete in regions covered by only a single plate.

Figure 14 shows the distribution of DR10 BOSS spectroscopy as a function of lookback time, or equivalently redshift. The galaxy distribution peaks at a redshift of 0.5 (about 5.5 Gyr ago), with very few galaxies above redshift 0.7. The majority of quasars lie between redshifts 2 and 3.5, by design: this is the regime in which the Lyman α forest enters the BOSS spectral coverage.

These distributions are shown in more detail in Figure 15, comparing the redshift distributions of galaxies and quasars to those from the SDSS-I/II Legacy survey. The SDSS-I/II galaxy survey included a magnitude-limited sample with median redshift $z \approx 0.10$ (Strauss et al. 2002), and a magnitude- and color-selected sample of luminous red galaxies extending to beyond $z = 0.4$ (Eisenstein et al. 2001). The SDSS-I/II quasar survey (Richards et al. 2002; Schneider et al. 2010) selects at all redshifts, and is flux-limited at magnitudes significantly brighter than BOSS, leading to the bulk of quasars below $z = 2$. Indeed, the BOSS DR10 galaxy sample is roughly the same size as the full DR7 Legacy galaxy sample (at almost five times the median redshift) and the BOSS DR10 quasar sample is significantly larger than its Legacy counterpart. DR10 includes about 60% of the full BOSS footprint, so the samples will grow appreciably further.

In what follows, Section 4.1 describes a new quasar target class for quasars selected using WISE data, Section 4.2 describes the minor updates to the BOSS spectroscopic pipeline

in DR10, and Section 4.3 discusses additions to measurements of parameters from galaxy spectra.

4.1. A New Quasar Target Class in DR10

Ross et al. (2012) describes the quasar target selection used in BOSS. DR10 includes one new quasar target class, `BOSS_WISE_SUPP`, which uses photometry from SDSS and WISE to select $z > 2$ quasars that the standard BOSS quasar target selection may have missed, and to explore the properties of quasars selected in the near-infrared.

These objects were required to have detections in the 3.6μm, 4.5μm, and 12μm bands, to be point sources in SDSS imaging, and were selected with the following color cuts:

$$(u - g) > 0.4 \text{ and} (g - r) < 1.3. \quad (3)$$

The requirement of a 12μm detection removes essentially all the stellar contamination, without any WISE color cuts.

There are 5,007 spectra from this sample in DR10, with a density of $\sim 1.5/\text{deg}^2$ over the $\sim 3,100$ deg^2 of new area added by BOSS in DR10. Almost 3000 of these objects are spectroscopically confirmed to be quasars, with redshifts up to $z = 3.8$. 999 of these objects have $z > 2.15$.

Given the use of WISE photometry in target selection, we have imported the WISE All-Sky Release catalog (Cutri et al. 2012) into the SDSS Catalog Archive Server (CAS), and performed an astrometric cross-match with $4''$ matching radius with the SDSS catalog objects. In preliminary tests we found no systematic shift between the WISE and SDSS astrometric systems; $4''$ extends well into the tail of the match distance distribution. In addition to the CASE, the results of this matching are made available as flat files in the Science Archive Server (SAS).

4.2. Updates to BOSS Data Processing

We have become aware of transient hot columns on the spectrograph CCDs. Because fiber traces lie approximately along columns, a bad column can adversely affect a large swath of a given spectrum. With this in mind, unusual-looking spectra associated with fibers 40, 556, and 834 and fibers immediately adjacent should be treated with suspicion; these objects are often erroneously classified as $z > 5$ quasars. We will improve the masking of these bad columns in future data releases.

We have identified 2748 objects whose astrometry is unreliable in the SDSS imaging due to unexpected physical excursions of the SDSS telescope while scanning. As a consequence, the fibers may be somewhat offset from the true position of the object, often missing it entirely (and thus giving no signal in the spectrum). The redshift determination of each object is accompanied by a warning flag, `ZWARNING`, which indicates that the results are not reliable (Table 2 of Dawson et al. 2013). Objects with bad astrometry are assigned bit 8, `BAD_TARGET` in `ZWARNING`.

4.3. Updates to BOSS Galaxy Stellar Population Parameters

Estimating stellar populations for galaxies from SDSS spectra continues to be an active field with different valid approaches. DR9 included two different stellar population estimates: "Portsmouth" stellar masses derived from the spectra and emission-line fluxes (Maraston et al. 2012), and "Wisconsin" principal component analysis (PCA) of the stellar populations using fits to the wavelength range $\lambda = 3700$–5500 Å (Chen et al. 2012).

In DR9, these models were calculated just for BOSS spectra; in DR10 they are extended to the $\sim 930,000$ galaxy spectra from SDSS-I/II. All stellar population calculations use the WMAP7 ΛCDM cosmology with $H_0 = 70$ km/s/Mpc, $\Omega_M = 0.274$, and $\Omega_\Lambda = 0.726$ (White et al. 2011).

In DR10, we also include results from the Granada Stellar Mass code (Montero-Dorta et al., in preparation) based on the publicly available "Flexible Stellar Population Synthesis" code of Conroy et al. (2009). The Granada FSPS code makes use of an extensive grid of composite stellar population models with varying star formation history (based on simple τ-models), metallicity and dust attenuation. The Granada FSPS galaxy product provides spectro-photometric stellar masses, ages, specific star formation rates, and other stellar population properties, along with corresponding errors, for 8 different configurations, which are generated by applying simple, physically motivated priors to the parent grid. The following configurations are given: including or not including dust, using Kroupa (2001) vs. Salpeter (1955) stellar initial mass function, and two different configurations for the formation time of the galaxy: either it formed within the first 2 Gyr following the Big Bang ($z \sim 3.25$), or the galaxy formed between the time of the Big Bang and two Gyr before the observed redshift of the galaxy. The Granada FSPS product follows a similar spectro-photometric SED fitting approach as that of the Portsmouth galaxy product, but using different stellar population synthesis models.

Due to a bug in the DR9 version of the Portsmouth code, the reported equivalent width

values were effectively reported in the observed frame (and were thus too high by a factor of $(1+z)$) and the continuum flux densities were too low by a factor of $(1+z)$ (Thomas et al. 2013). These errors been corrected in the DR10 versions, which quotes EW and continuum density flux values each correctly in the restframe.

The Portsmouth code results in DR10 now include the full stellar mass probability distribution function for each spectrum.

The Wisconsin PCA code in DR9 used the stellar population model of Bruzual & Charlot (2003). In DR10, we have added the stellar population synthesis model of Maraston & Strömbäck (2011).

In addition, the covariance matrix in the flux density in neighboring pixels due to errors in spectrophotometry has been updated by using all of the repeat galaxy observations in DR10, rather than the 5,000 randomly selected repeat galaxy observations used in DR9. This covariance is important in fitting stellar population models to the spectra.

5. Data Distribution

All Data Release 10 data are available through data access tools linked from the DR10 web site.[6] The data are stored both as flat files in the Science Archive Server (SAS), and as a searchable database in the Catalog Archive Server (CAS). Both of these data servers have front-end web interfaces, called the "SAS Webapp"[7] and "SkyServer"[8] respectively. While the APOGEE data present a new type of data for SDSS (high-resolution near-infrared spectra), we have provided tools analogous to the existing SDSS tools. A number of different interfaces are available, each designed to accomplish a specific task.

- Color images of regions of the sky in JPEG format (based on the g, r and i images; see Lupton et al. 2004) can be viewed in a web browser with the SkyServer Navigate tool. With DR10 we have added the ability to view 2MASS images to complement the APOGEE spectra.
- FITS images can be searched for, viewed and downloaded through the SAS Webapp.

[6]http://www.sdss3.org/dr10/

[7]http://data.sdss3.org/

[8]http://skyserver.sdss3.org/dr10/

- Complete catalog information (astrometry, photometry, etc.) of any imaging object can be viewed through the SkyServer Explore tool.
- Individual spectra, both optical and infrared, can be searched for, viewed and downloaded through the SAS Webapp.
- Catalog search tools are available through the SkyServer interface to the CAS, each of which returns catalog data for objects that match supplied criteria. For more advanced queries, a powerful and flexible catalog search website called "CasJobs" allows users to create their own personalized data sets and then to modify or graph their data.

Links to all of these methods are provided at http://www.sdss3.org/dr10/data_access/.

The DR10 web site also features data access tutorials, a glossary of SDSS terms, and detailed documentation about algorithms used to process the imaging and spectroscopic data and select spectroscopic targets.

Imaging and spectroscopic data from all prior data releases are also available through DR10 data access tools.

6. Conclusions

The SDSS-III project will present two more public data releases: DR11 and DR12, both to be released in December 2014. DR11 will include data taken through the summer of 2013. DR12 will be the final SDSS-III data release and will include the final data from all observations with APOGEE, BOSS, MARVELS, and SEGUE-2.

In July 2014, operation of the 2.5-m Sloan Foundation Telescope will be taken over by the next-generation SDSS, currently known as SDSS-IV, which plans to operate for six years. SDSS-IV consists of three surveys mapping the Milky Way Galaxy, the nearby galaxy population, and the distant universe. APOGEE-2 will continue the current APOGEE program of targeting Milky Way stars to study Galactic archaeology and stellar astrophysics. It will include a southern component, observing from the 2.5m du Pont Telescope at Las Campanas Observatory, Chile, in order to map the Milky Way as a whole. Mapping Nearby Galaxies at APO (MaNGA) will use the BOSS spectrograph in a new mode, bundling fibers into integral field units to observe 10,000 nearby galaxies with spatially resolved spectroscopy. MaNGA has already successfully tested its planned hardware configuration using BOSS time within SDSS-III for a small number of targets. Finally, the Extended Baryon Oscillation Spectroscopic Survey (eBOSS) will create the largest volume three-dimensional map of the

universe to date, in order to measure baryon acoustic oscillations and constrain cosmological parameters in the critical and largely unexplored redshift range $0.6 < z < 2.1$.

SDSS-III Data Release 10 makes use of data products from the Two Micron All Sky Survey, which is a joint project of the University of Massachusetts and the Infrared Processing and Analysis Center/California Institute of Technology, funded by the National Aeronautics and Space Administration and the National Science Foundation.

SDSS-III Data Release 10 makes use of data products from the Wide-field Infrared Survey Explorer, which is a joint project of the University of California, Los Angeles, and the Jet Propulsion Laboratory/California Institute of Technology, funded by the National Aeronautics and Space Administration.

Funding for SDSS-III has been provided by the Alfred P. Sloan Foundation, the Participating Institutions, the National Science Foundation, and the U.S. Department of Energy Office of Science. The SDSS-III web site is http://www.sdss3.org/.

SDSS-III is managed by the Astrophysical Research Consortium for the Participating Institutions of the SDSS-III Collaboration including the University of Arizona, the Brazilian Participation Group, Brookhaven National Laboratory, Carnegie Mellon University, University of Florida, the French Participation Group, the German Participation Group, Harvard University, the Instituto de Astrofisica de Canarias, the Michigan State/Notre Dame/JINA Participation Group, Johns Hopkins University, Lawrence Berkeley National Laboratory, Max Planck Institute for Astrophysics, Max Planck Institute for Extraterrestrial Physics, New Mexico State University, New York University, Ohio State University, Pennsylvania State University, University of Portsmouth, Princeton University, the Spanish Participation Group, University of Tokyo, University of Utah, Vanderbilt University, University of Virginia, University of Washington, and Yale University.

REFERENCES

Abazajian, K., et al. 2004, AJ, 128, 502

Abazajian, K., et al. 2005, AJ, 129, 1755

Abazajian, K., et al. 2003, AJ, 126, 2081

Abazajian, K. N., et al. 2009, ApJS, 182, 543

Adelman-McCarthy, J. K., et al. 2008, ApJS, 175, 297

Adelman-McCarthy, J. K., et al. 2007, ApJS, 172, 634

Adelman-McCarthy, J. K., et al. 2006, ApJS, 162, 38

Ahn, C. P., et al. 2012, ApJS, 203, 21

Aihara, H., et al. 2011, ApJS, 193, 29

Anderson, L., et al. 2013, ArXiv e-prints

Anderson, L., et al. 2012, MNRAS, 427, 3435

Annis, J., et al. 2011, ArXiv e-prints

Benjamin, R. A., et al. 2003, PASP, 115, 953

Bolton, A. S., et al. 2012, AJ, 144, 144

Borucki, W. J., et al. 2010, Science, 327, 977

Bruzual, G., & Charlot, S. 2003, MNRAS, 344, 1000

Busca, N. G., et al. 2013, A&A, 552, A96

Chaplin, W. J., et al. 2013, ApJ, 766, 101

Chen, Y.-M., et al. 2012, MNRAS, 421, 314

Churchwell, E., et al. 2009, PASP, 121, 213

Conroy, C., Gunn, J. E., & White, M. 2009, ApJ, 699, 486

Cutri, R. M., et al. 2012, 1

Dawson, K. S., et al. 2013, AJ, 145, 10

Eisenstein, D. J., et al. 2001, AJ, 122, 2267

Eisenstein, D. J., et al. 2011, AJ, 142, 72

Frieman, J. A., et al. 2008, AJ, 135, 338

Garcia-Perez, A., et al. 2013, *in prep*

Garnett, J. D., et al. 2004, in Society of Photo-Optical Instrumentation Engineers (SPIE) Conference Series, Vol. 5499, Society of Photo-Optical Instrumentation Engineers (SPIE) Conference Series, ed. J. D. Garnett & J. W. Beletic, 35–46

Gilliland, R. L., et al. 2010, PASP, 122, 131

Gunn, J. E., et al. 1998, AJ, 116, 3040

Gunn, J. E., et al. 2006, AJ, 131, 2332

Hekker, S., et al. 2011, A&A, 530, A100

Indebetouw, R., et al. 2005, ApJ, 619, 931

Ivezić, Ž., et al. 2004, Astronomische Nachrichten, 325, 583

Komatsu, E., et al. 2011, ApJS, 192, 18

Kroupa, P. 2001, MNRAS, 322, 231

Lupton, R., Blanton, M. R., Fekete, G., Hogg, D. W., O'Mullane, W., Szalay, A., & Wherry, N. 2004, PASP, 116, 133

Lupton, R., Gunn, J. E., Ivezić, Z., Knapp, G. R., & Kent, S. 2001, in Astronomical Society of the Pacific Conference Series, Vol. 238, Astronomical Data Analysis Software and Systems X, ed. F. R. Harnden, Jr., F. A. Primini, & H. E. Payne, 269

Majewski, S. R., Zasowski, G., & Nidever, D. L. 2011, ApJ, 739, 25

Majewski, S. R., et al. 2013, *in prep*

Maraston, C., et al. 2012, ArXiv e-prints, 1207.6114

Maraston, C., & Strömbäck, G. 2011, MNRAS, 418, 2785

Mészáros, S., et al. 2012, AJ, 144, 120

Mészáros, S., et al. 2013, *submitted*

Nidever, D., et al. 2013, *in prep*

Padmanabhan, N., et al. 2008, ApJ, 674, 1217

Pâris, I., et al. 2013, *in prep*

Pier, J. R., Munn, J. A., Hindsley, R. B., Hennessy, G. S., Kent, S. M., Lupton, R. H., & Ivezić, Ž. 2003, AJ, 125, 1559

Pinsonneault, M., et al. 2013, *in prep*

Richards, G. T., et al. 2002, AJ, 123, 2945

Ross, N. P., et al. 2012, ApJS, 199, 3

Salpeter, E. E. 1955, ApJ, 121, 161

Schneider, D. P., et al. 2010, AJ, 139, 2360

Shetrone, M., et al. 2013, *in prep*

Skrutskie, M. F., et al. 2006, AJ, 131, 1163

Smee, S., Gunn, J. E., Uomoto, A., Roe, N., Schlegel, D., Rockosi, C. M., Carr, M. A., Leger, F., Dawson, K. S., Olmstead, M. D., Brinkmann, J., Owen, R., Barkhouser, R. H., Honscheid, K., Harding, P., Long, D., Lupton, R. H., Loomis, C., Anderson, L., Annis, J., Bernardi, M., Bhardwaj, V., Bizyaev, D., Bolton, A. S., Brewington, H., Briggs, J. W., Burles, S., Burns, J. G., Castander, F., Connolly, A., Davenport, J. R., Ebelke, G., Epps, H., Feldman, P. D., Friedman, S., Frieman, J., Heckman, T., Hull, C. L., Knapp, G. R., Lawrence, D. M., Loveday, J., Mannery, E. J., Malanushenko, E., Malanushenko, V., Merrelli, A., Muna, D., Newman, P., Nichol, R. C., Oravetz, D., Pan, K., Pope, A. C., Ricketts, P. G., Shelden, A., Sandford, D., Siegmund, W., Simmons, A., Smith, D., Snedden, S., Schneider, D. P., Strauss, M., SubbaRao, M., Tremonti, C., Waddell, P., & York, D. G. 2013, AJ, *in press*

Stoughton, C., et al. 2002, AJ, 123, 485

Strauss, M. A., et al. 2002, AJ, 124, 1810

Thomas, D., et al. 2013, MNRAS, 431, 1383

Tucker, D. L., et al. 2006, Astronomische Nachrichten, 327, 821

Wells, D. C., Greisen, E. W., & Harten, R. H. 1981, A&AS, 44, 363

White, M., et al. 2011, ApJ, 728, 126

Wilson, J. C., et al. 2013, *in prep*

Wright, E. L., et al. 2010, AJ, 140, 1868

Yanny, B., et al. 2009, AJ, 137, 4377

York, D. G., et al. 2000, AJ, 120, 1579

Zasowski, G., et al. 2013, *submitted*

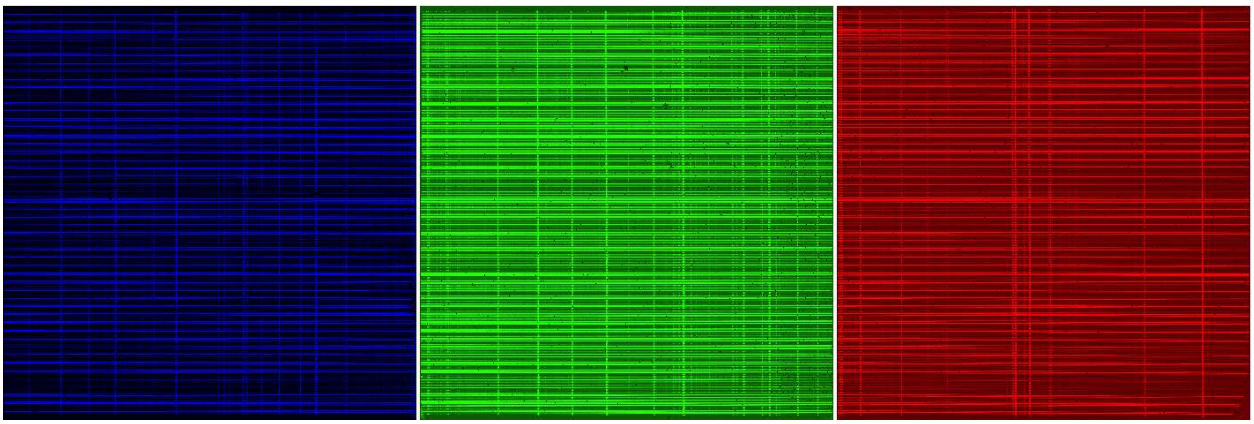

Fig. 4.— A 2D spectrum from the APOGEE instrument. The three chips are shown with wavelength increasing to the right. Each fiber is imaged onto several pixels (vertically). The gaps shown in this image are slightly smaller than in the detector. Note the vertical series of points from sky lines, and the horizontal rows showing bright stars, faint stars, and sky fibers. MWV: Consider also showing a zoom of a region. Say 20 fibers?

Fig. 5.— Examples of "typical" APOGEE spectra, showing the range of qualities. SCHIAVON and HOLTZMAN will prepare TODO. May end up being redundant with Figure 10?

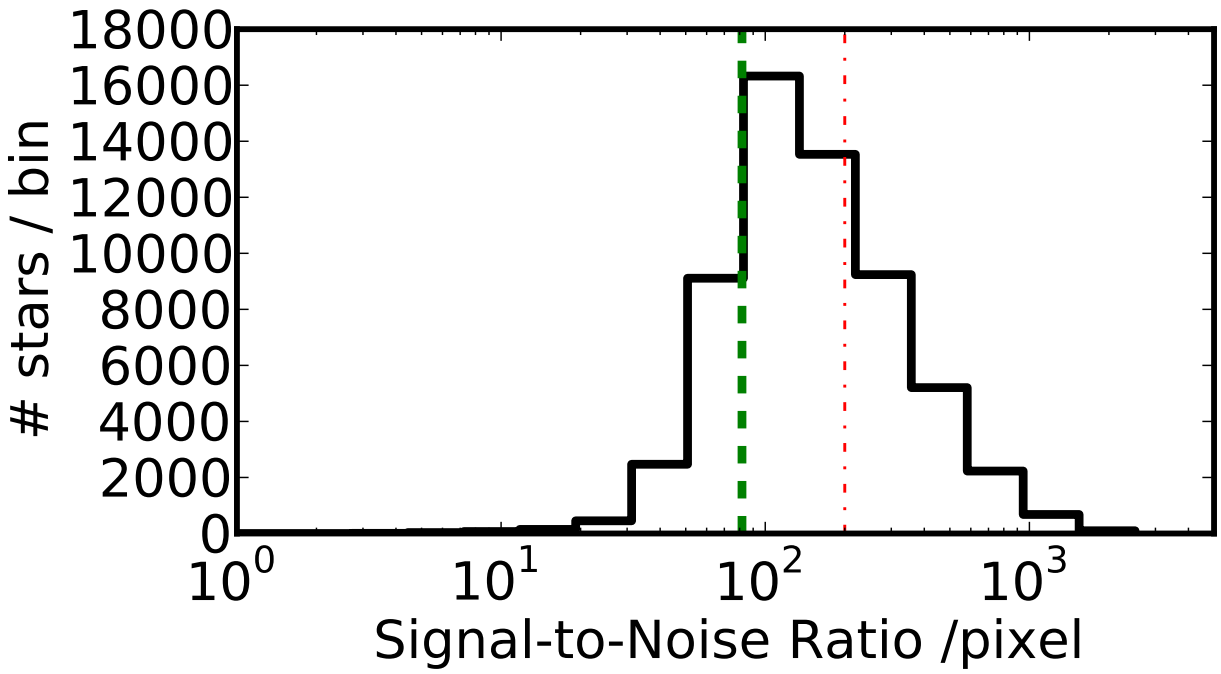

Fig. 6.— Reported S/N per pixel of APOGEE DR10 co-added stellar spectra. Current measurements of repeated observations imply that there is a practical limit of S/N $\sim$ 200 in the co-added spectra, shown as the dot-dashed line. The dashed line denotes the target S/N $\sim$ 100 per resolution element goal, corresponding to S/N $\sim$ 80 per pixel.

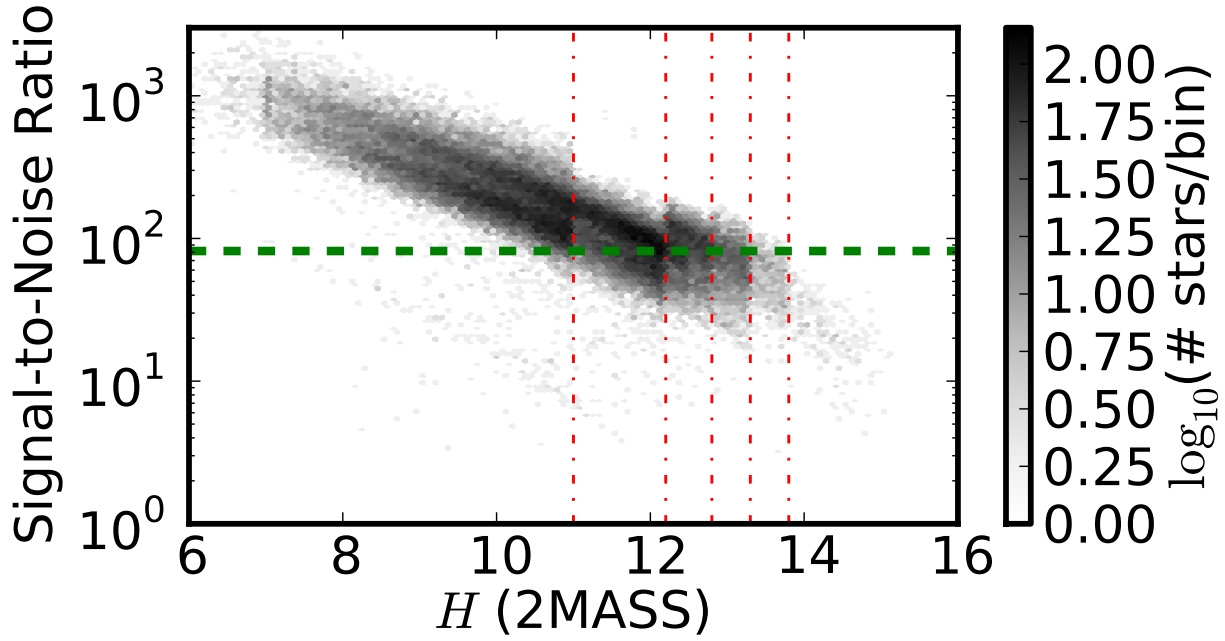

Fig. 7.— S/N per pixel of spectra of stars as a function of their apparent H-band magnitude (density is on a log scale). The vertical dot-dashed lines indicate the magnitude limits for stars in each bin of intended number of visits: 1, 3, 6, 12, 24 visits for $H = 11.0$, 12.2, 12.8, 13.3, and 13.8 mag. The horizontal dashed line indicates the target S/N $\sim$ 100 per resolution element.

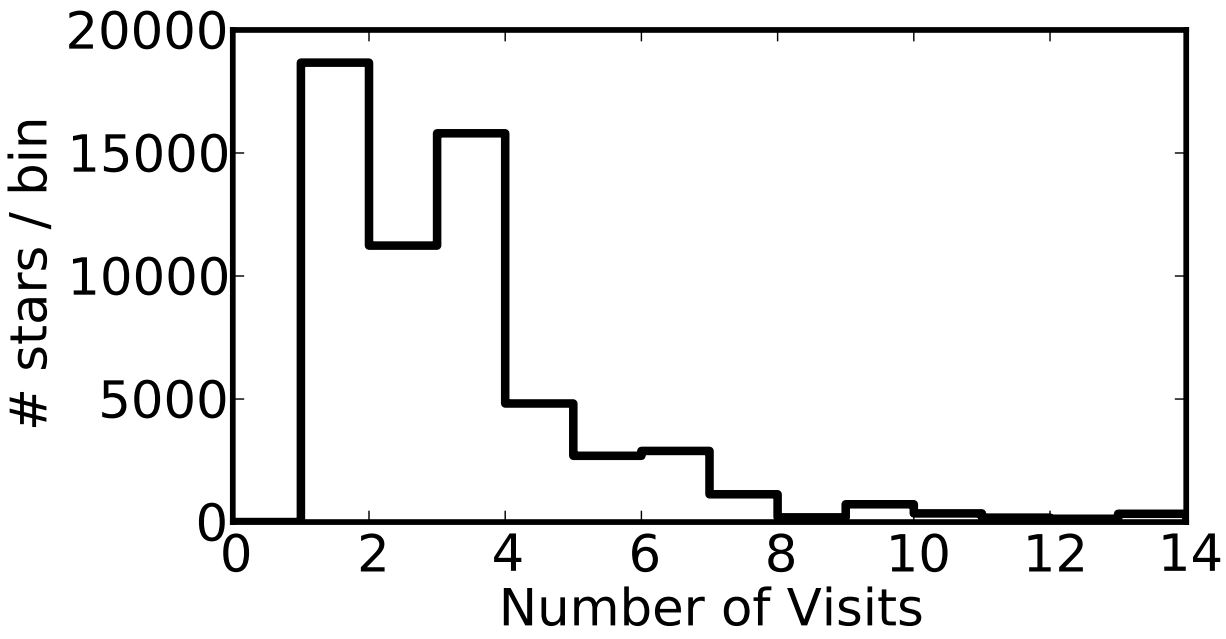

Fig. 8.— The distribution of number of spectroscopic visits for APOGEE stars included in DR10. While the bulk of stars have three or fewer visits, they may have reached our spectral S/N requirement if they are bright enough; see Figure 7

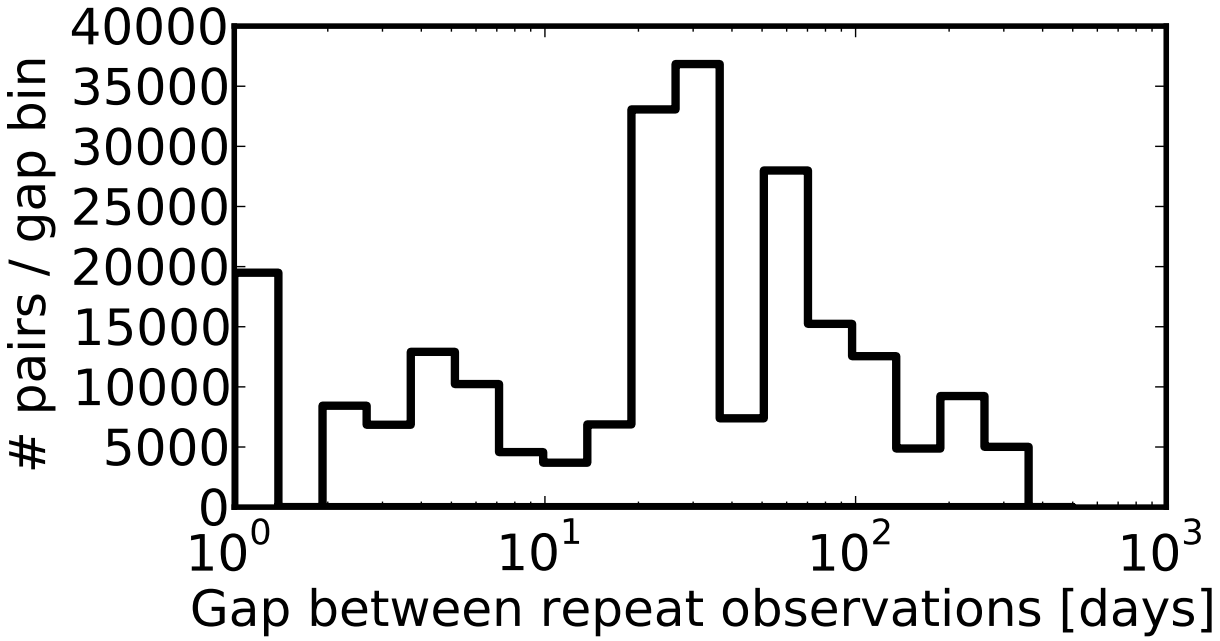

Fig. 9.— The distribution of time between visits for APOGEE stars, useful for determining the sensitivity to radial velocity variations due to binarity. This quantity is the absolute value of the time difference for all unique pairs of observations for each star. The most prominent peaks are at one and two months.

Fig. 10.— Figures showing ASPCAP fits to observed spectra in a range of Teffs and metallicities should be included. SCHIAVON and HOLTZMAN will prepare

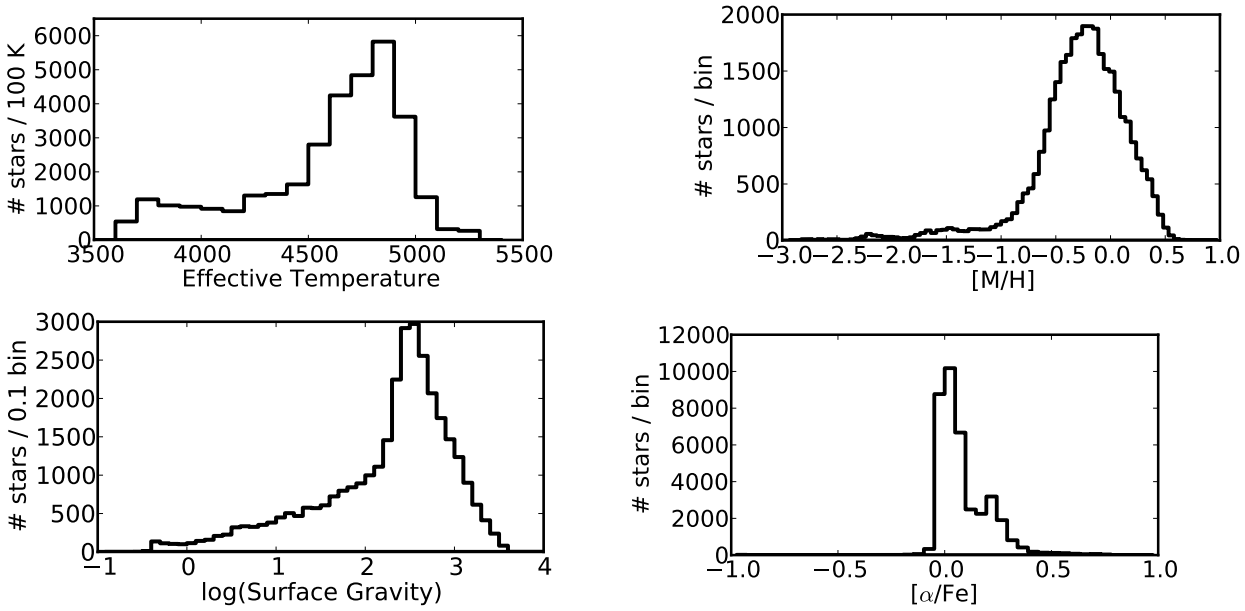

Fig. 11.— One-dimensional distributions of quantities measured by ASPCAP of DR10 stars: temperatures, surface gravities, metallity, and [α/Fe].

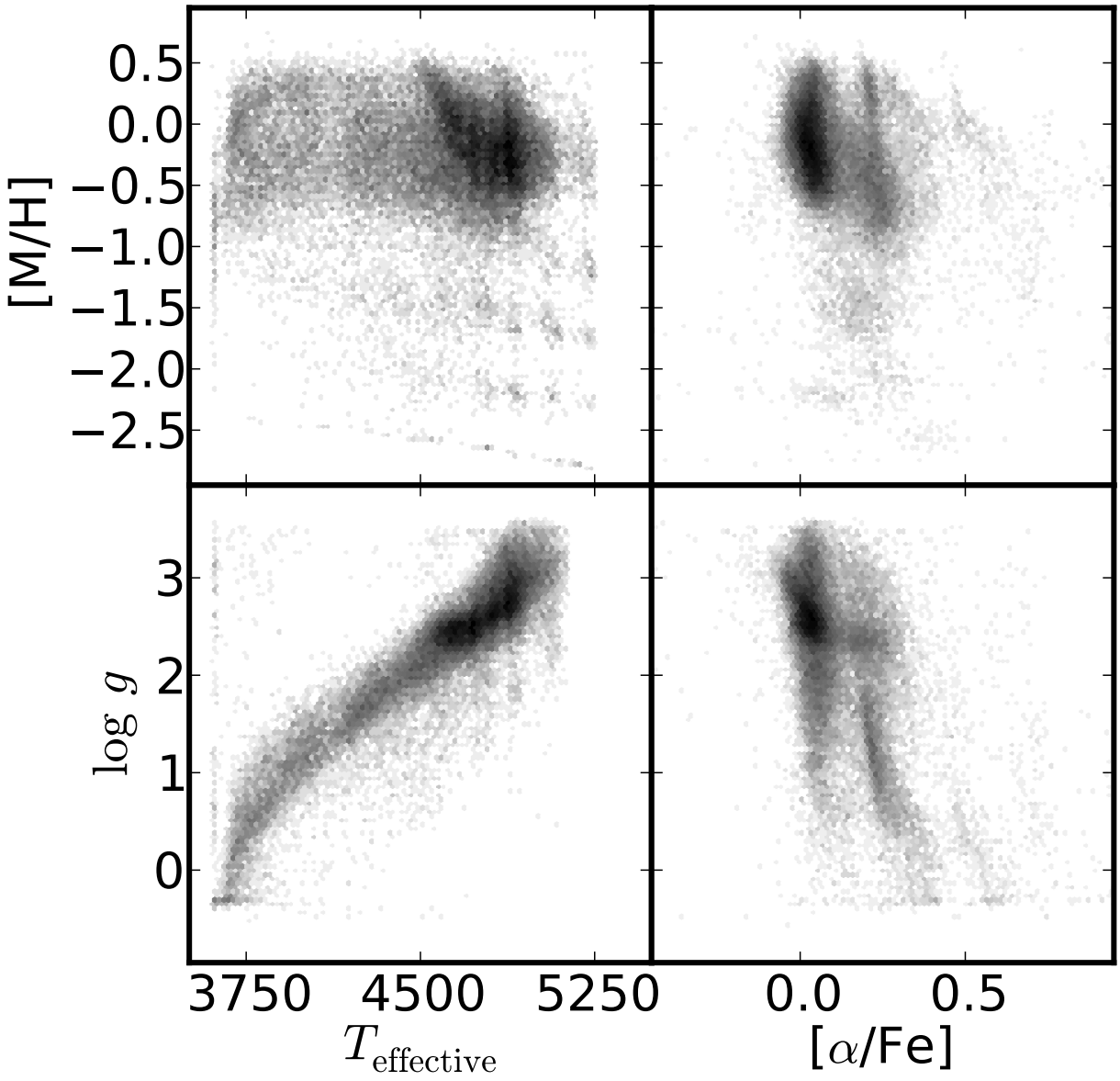

Fig. 12.— Correlations between the quantities shown in Figure 11. The star counts in each two-dimensional bin are on a logarithmic scale. MWV: Make and use consistent Color bar.

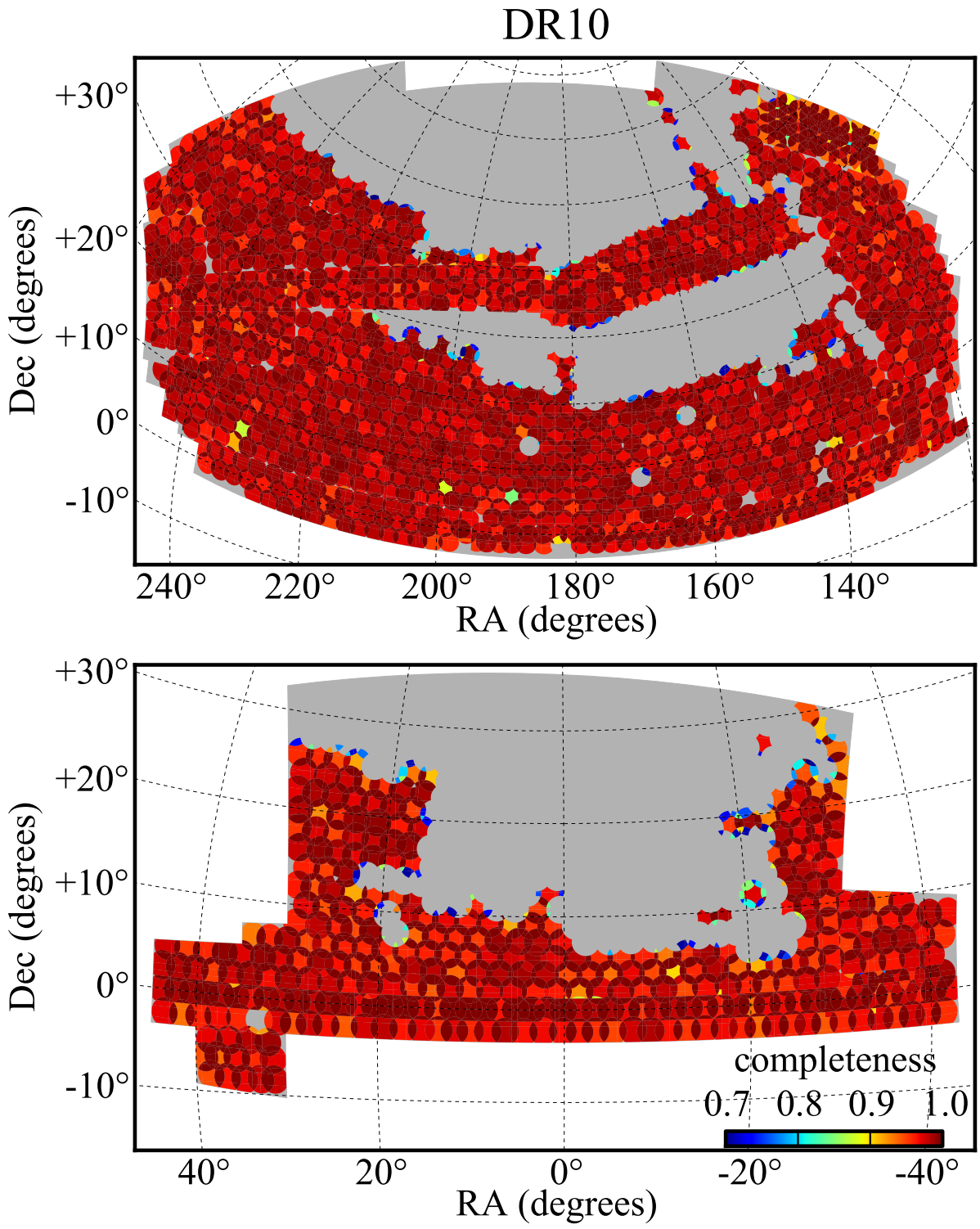

Fig. 13.— BOSS DR10 spectroscopic sky coverage in the Northern Galactic Cap (top) and Southern Galactic Cap (bottom). The grey region is the ultimate coverage goal by the end of the survey, totaling 10,000 deg^2. The color coding indicates the fraction of CMASS galaxy targets that receive a fiber; the fact that no two fibers can be placed closer than 62″ on a given plate keeps the completeness from being 100%. Note the higher completeness on the Equator in the Southern Galactic Cap (Stripe 82).

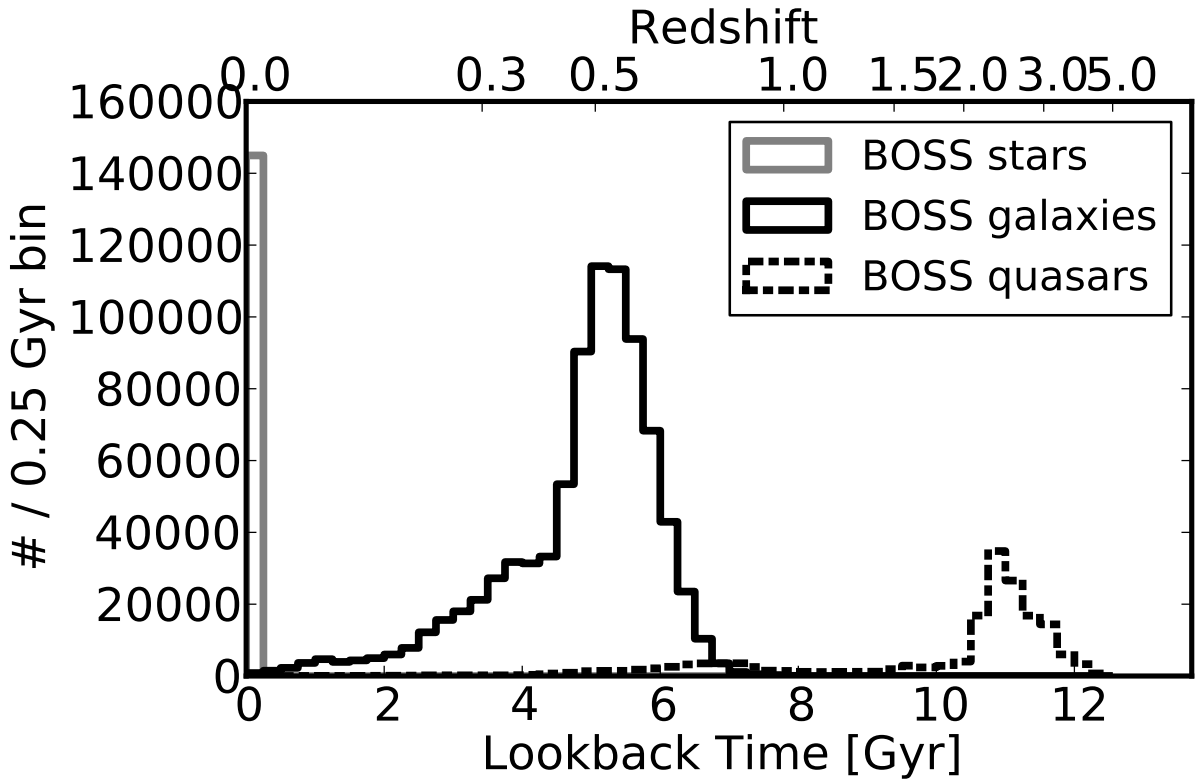

Fig. 14.— The distribution of BOSS DR10 objects versus lookback time for the 144,968 unique stars; 859,322 unique galaxies; and 166,300 quasars. Lookback time is based on the observed redshift under the assumption of a flat ΛCDM cosmology $(\Omega_M, \Omega_\Lambda, h) = (0.272, 0.728, 0.71)$, consistent with the joint cosmological analysis of WMAP7 (Komatsu et al. 2011). This figure is practically identical to the equivalent Fig. 3 in Ahn et al. (2012), scaled up by a factor of 1.8.

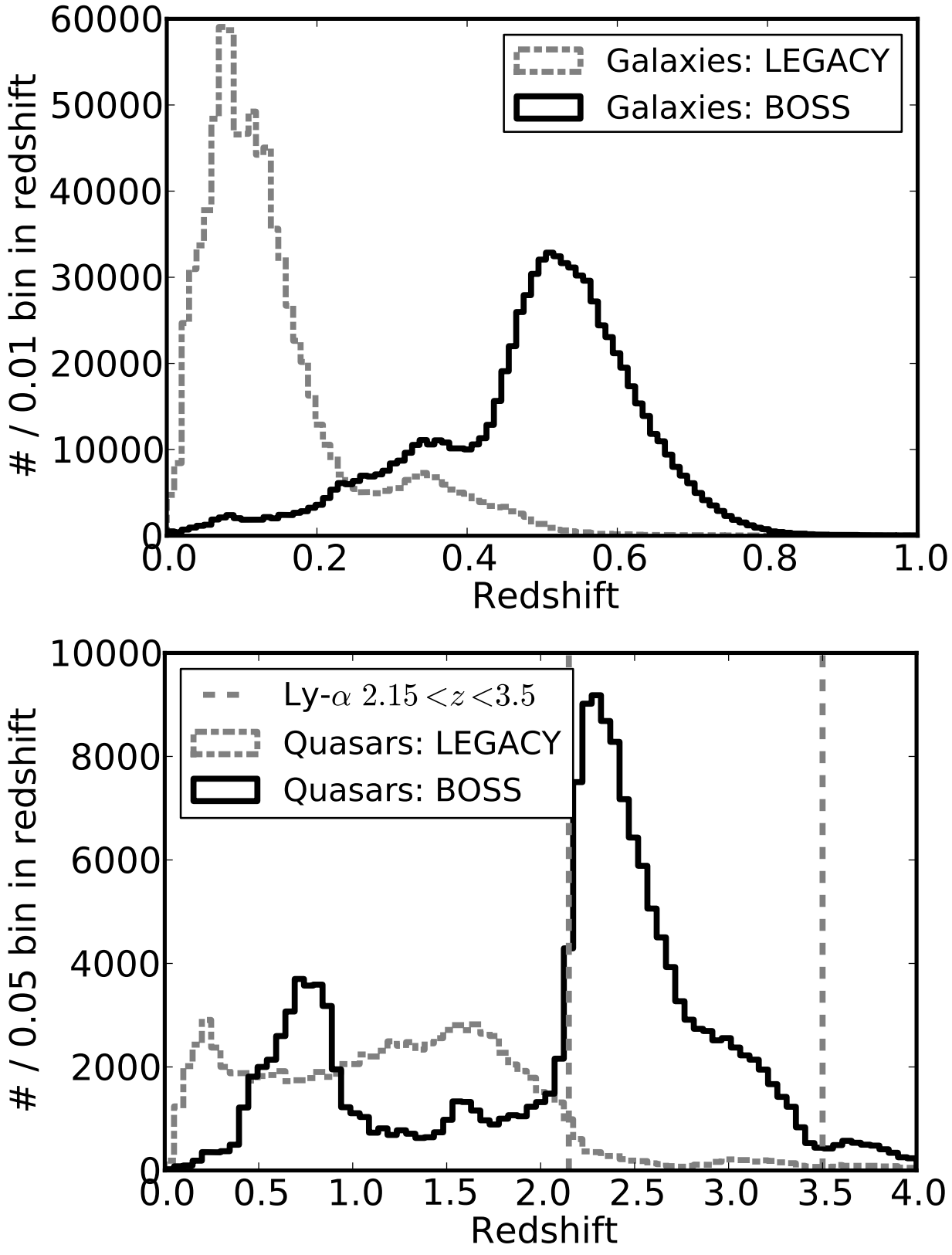

Fig. 15.— $N(z)$ of SDSS-III BOSS spectra in DR10 compared to that of the SDSS-I/II Legacy spectra for galaxies (top) and quasars (bottom).